

Statistical summaries of unlabelled evolutionary trees and ranked hierarchical clustering trees

Rajanala Samyak¹ and Julia A. Palacios^{1,2,*}

¹Department of Statistics, Stanford University, Stanford, CA 94305, USA

²Department of Biomedical Data Science, Stanford Medicine, Stanford, CA 94305, USA

*Corresponding author email: juliapr@stanford.edu

June 8, 2021

Abstract

Rooted and ranked binary trees are mathematical objects of great importance used to model hierarchical data and evolutionary relationships with applications in many fields including evolutionary biology and genetic epidemiology. Bayesian phylogenetic inference usually explore the posterior distribution of trees via Markov Chain Monte Carlo methods, however assessing uncertainty and summarizing distributions or samples of such trees remains challenging. While labelled phylogenetic trees have been extensively studied, relatively less literature exists for unlabelled trees which are increasingly useful, for example when one seeks to summarize samples of trees obtained with different methods, or from different samples and environments, and wishes to assess stability and generalizability of these summaries. In our paper, we exploit recently proposed distance metrics of unlabelled ranked binary trees and unlabelled ranked genealogies (equipped with branch lengths) to define the Fréchet mean and variance as summaries of these tree distributions. We provide an efficient combinatorial optimization algorithm for computing the Fréchet mean from a sample of or distribution on unlabelled ranked tree shapes and unlabelled ranked genealogies. We show the applicability of our summary statistics for studying popular tree distributions and for comparing the SARS-CoV-2 evolutionary trees across different locations during the COVID-19 epidemic in 2020.

Keywords: Binary trees; Combinatorial optimization; Evolutionary trees; Fréchet; Summarizing trees; Unlabelled trees.

1 Introduction

Binary trees are used to represent the ancestral relationships of samples in evolving populations and to model other type of dependent data that is the result of tree-like structures, such as transmission trees. In phylogenetics, population genetics, and cell biology, evolutionary trees are inferred from observed molecular

sequence data or from observed evolutionary traits in a sample of individuals from a population. These individuals can be viral sequences from infected hosts (viral phylodynamics), species (phylogenetics), individuals from a single species (population genetics), or cells (cancer evolution). The estimated tree describes the inferred ancestral relationships of the samples and provides information about the past evolutionary dynamics of the sample’s population. For example, in the context of viral phylodynamics, the tree provides information about the past transmission history and pathogenesis [Volz et al., 2013].

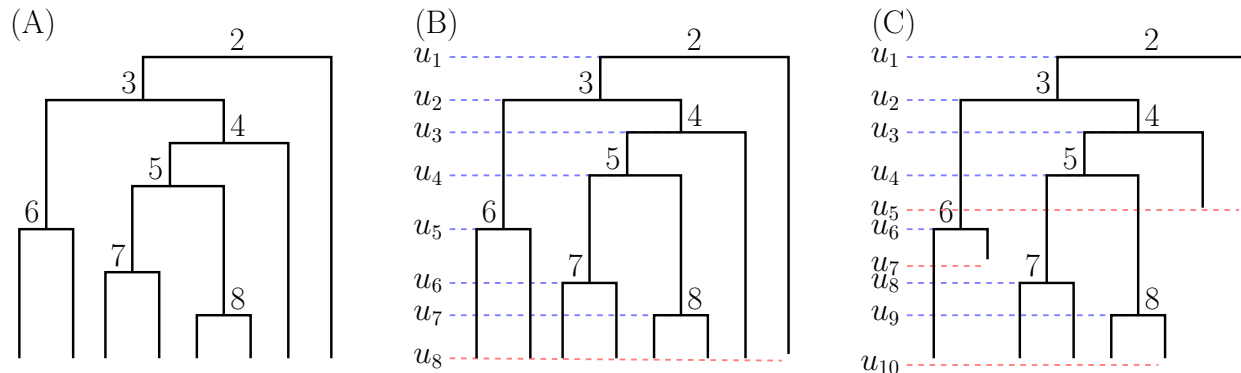


Figure 1: **Tree examples.** (A) isochronous ranked tree shape (topology only); (B) isochronous ranked genealogies (ranked tree shape and branching times); and (C) heterochronous ranked genealogy with different sampling times (red dashed lines).

Distance-based summaries of labelled and unranked tree structures have been extensively studied such as phylogenetic trees [Hillis et al., 2005, Chakerian and Holmes, 2012, Benner and Bačák, 2013, Willis and Bell, 2018, Brown and Owen, 2019], and hierarchical clustering trees such as CART [Breiman, 1984] in the last few decades. These summaries rely on metrics such as the BHV distance [Billera et al., 2001] defined on tree space. Kuhner and Yamato [2014] presents a comparison of different distances on such space. In the case of labelled trees, it is usually assumed that all sampled trees have the same set of leaves (labels). Other type of summaries of labelled and unranked trees include bootstrap confidence levels [Felsenstein, 1985, Efron et al., 1996], and maximum clade credibility trees [Heled and Bouckaert, 2013, O’Reilly and Donoghue, 2018].

In this article, we are interested in summarizing different tree structures, namely those that are ranked and unlabelled. These trees are useful in the study of the ancestral relationships of a sample of objects which are exchangeable. One potential area of application is in the study of cancer evolution where the tree represents the evolutionary history of many cells in a patient’s tumor. We may want to summarize many such trees, each tree inferred from a different patient, in order to find a “representative” tree and quantify how much variation or heterogeneity is present across patients with the same type of cancer or across different types of cancer. Similar type of questions have been studied assuming a coarser type of tree structure [Govek et al., 2018]. Another application is in infectious disease transmission, where we study the mutation history of different viral sequences. Here, we compute summary statistics from samples of SARS-CoV-2 trees using RNA sequences available in the data repository GISAID between February and September 2020.

Recent mathematical results concerning distance metrics on the space of ranked evolutionary trees without leaf labels enable quantitative comparisons of evolutionary trees of different sets of organisms living at

different geographic locations and different time periods. These metrics have been used for comparing posterior distributions (and testing for distribution equality) of trees of human influenza A virus from two different geographic regions; for summarizing empirical distributions via medoids; and for defining credible sets of posterior distributions [Kim et al., 2019].

In this article, we use the previously defined distance metrics on unlabelled ranked evolutionary trees to understand distributional properties of some popular tree models used in Biology and to summarize samples of trees. Tree samples can be either obtained from the posterior distribution for a given sample of molecular sequences such as those obtained with BEAST [Suchard et al., 2018], or trees independently obtained in different studies.

A recently proposed Bayesian method for inferring evolutionary parameters from molecular data is based on the Tajima coalescent for unlabelled ranked evolutionary trees [Palacios et al., 2019, Cappello et al., 2020]. This method approximates the posterior distribution of model parameters and evolutionary trees by Markov chain Monte Carlo methods (MCMC). While summarizing real-valued parameters is straightforward, summarizing a posterior sample of unlabelled ranked evolutionary trees is more challenging. As discussed above, methods for summarizing posterior samples of labelled evolutionary trees exist [Heled and Bouckaert, 2013, Benner and Bačák, 2013, Brown and Owen, 2019]. However, we are not aware of methods applicable for summarizing posterior samples of unlabelled ranked trees.

To summarize samples and populations of unlabelled ranked evolutionary trees, we define the sample and population Fréchet means and variances in terms of the recently proposed d_1 and d_2 distances. We compare these summaries to other measures of centrality and dispersion on the same space. We show that finding the Fréchet mean consists in finding the solution of an integer programming problem. However, the search space of ranked evolutionary trees grows super-exponentially in n , the number of leaves, which makes the problem of finding the Fréchet mean computationally challenging for large values of n . For large n , we rely on stochastic combinatorial optimization, and propose a simulated annealing algorithm for estimating the Fréchet mean in the case of both isochronous and heterochronous ranked tree shapes. The time complexity for computation of these trees is independent of N , the number of trees, and instead only depends on n , the number of leaves in each tree. The advantage of our approach is that the output is not restricted to the sample, and can be any element of the space.

We also introduce exploratory tools for the space of unlabelled ranked trees such as a total ordering, a Markov chain on the space, and credible balls. These are used in various analyses in this paper but also can also merit separate study.

In Section 2 we formally define the class of evolutionary trees considered, show how these trees are in bijection with a particular set of triangular matrices of integers, and show how to compute the distance metrics proposed in [Kim et al., 2019]. Section 3 introduces the Fréchet mean as a summary of location and methods for computing and approximating it, including a simulated annealing algorithm using a Markov chain for state space exploration. In Section 4 we describe the Fréchet variance as a statistic of spread for a given sample or distribution. In Section 5 we compare various summary statistics of theoretical distributions as well as empirical simulated distributions. As a real data example, we analyse the posterior distributions of evolutionary trees inferred from SARS-CoV-2 molecular sequences from the states of California, Texas,

Florida, and Washington. We obtain Fréchet mean trees for different samples and display multidimensional scaling plots to visualize intra-state and inter-state variability. In Section 7, we conclude and discuss future directions.

We have developed an R package, `FMATRIX` (github.com/RSamyak/fmatrix), which implements the various methods discussed in this paper. The package is compatible with `PHYLODYN` [Karcher et al., 2017], an R package for phylodynamic simulation and inference, and `APE` [Paradis and Schliep, 2019], an R package to handle phylogenetic trees.

2 Preliminaries

Ranked unlabelled trees or *ranked tree shapes* are rooted binary trees, with an increasing ordering of the interior nodes. They are *unlabelled* in the sense that the external nodes (leaves) are unlabelled. We however rank the internal nodes, starting at the root with label 2 (Figure 1 (A)). A ranked unlabelled tree, additionally equipped with the vector of branching times is called a *ranked genealogy* (Figure 1 (B)).

A ranked unlabelled tree (or ranked genealogy) is called *isochronous* if all the leaves are sampled at the same time, usually assumed to be sampled at time 0 (Figure 1 (A-B)). In applications of rapidly evolving pathogens such as Influenza A virus, molecular sequences (leaves) are sampled at different times (Figure 1 (C)) and these trees are called *heterochronous*.

Recently, Kim et al. [2019] proposed metrics on the space of ranked tree shapes and ranked genealogies for comparing and assessing differences between tree distributions. The utility of the metrics was demonstrated in a series of simulation studies to assess differences between the posterior distributions of ranked genealogies of Influenza A virus obtained from two different geographic regions. The proposed metrics rely on a unique representation of ranked tree shapes as triangular matrices of integers, called **F**-matrices. The distances between two ranked unlabelled trees are then calculated as L_1 and L_2 distances between these matrices (Eqs. 1 and 2). A formal definition of **F**-matrices is given in Theorem 1.

For a given isochronous ranked tree shape with n leaves, we denote the time of a branching event at each node i by u_{i-1} and the time interval between the two subsequent nodes i and $i + 1$ by $I_i = (u_{i-1}, u_i)$. For convenience, we assign $u_n = 0$ at the leaves. An **F**-matrix representation of a ranked tree shape with n leaves is an $(n - 1) \times (n - 1)$ triangular matrix of non-negative integers. The diagonal elements of the **F**-matrix indicate the number of branches at each time interval. The off-diagonal element $F_{i,j}$, $2 \leq j < i \leq n - 1$, represents the number of branches extant at $I_j = (u_{j+1}, u_j)$ that do not bifurcate during the interval (u_{i+1}, u_j) . Figure 2 shows all ranked tree shapes with 5 leaves (first row) and their corresponding **F**-matrix encodings (second row).

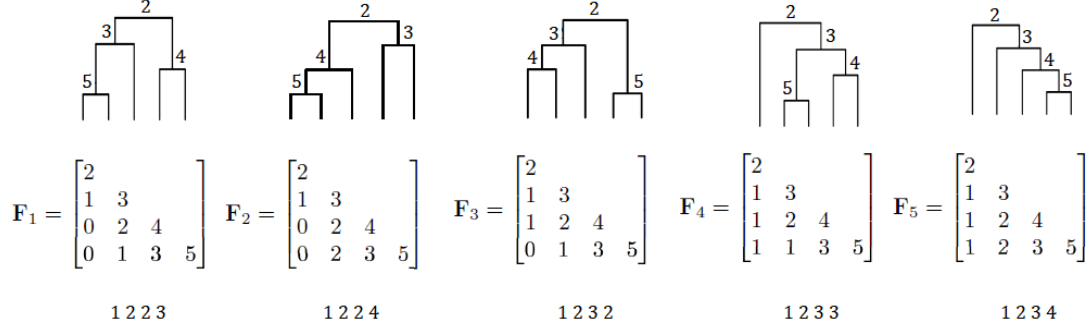


Figure 2: **All ranked tree shapes with $n = 5$ leaves.** The second row shows the corresponding \mathbf{F} -matrix representation of the ranked tree shape of the first row, and the third row shows their corresponding functional code representations (see section D of the appendix).

Theorem 1. The space of ranked tree shapes with n leaves \mathcal{T}_n is in bijection with the space \mathcal{F}_n of $(n - 1) \times (n - 1)$ \mathbf{F} -matrices, which are lower triangular square matrices of non-negative integers that obey the following constraints:

1. The diagonal elements are $F_{i,i} = i + 1$ for $i = 1, \dots, n - 1$ and the subdiagonal elements are $F_{i+1,i} = i$ for $i = 1, \dots, n - 2$.
2. The elements $F_{i,1}$, $i = 3, \dots, n - 1$, in the first column satisfy $\max\{0, F_{i-1,1} - 1\} \leq F_{i,1} \leq F_{i-1,1}$.
3. All the other elements $F_{i,k}$, $i = 4, \dots, n - 1$ and $k = 2, \dots, i - 2$ satisfy the following inequalities:

$$\begin{aligned}
 \max\{0, F_{i,k-1}\} &\leq F_{i,k} \\
 F_{i-1,k} - 1 &\leq F_{i,k} \leq F_{i-1,k} \\
 F_{i,k-1} + F_{i-1,k} - F_{i-1,k-1} - 1 &\leq F_{i,k} \leq F_{i,k-1} + F_{i-1,k} - F_{i-1,k-1}
 \end{aligned}$$

The proof is in the appendix, in Section B.

Given two ranked tree shapes y_1 and $y_2 \in \mathcal{T}_n$, with corresponding \mathbf{F} -matrices F_1 and F_2 , d_1 and d_2 are the L_1 and the L_2 distances on the space of matrices, restricted to \mathcal{F}_n , the class of \mathbf{F} -matrices, that is

$$d_1(y_1, y_2) := d_1(F_1, F_2) = \sum_{i,j} |(F_1)_{ij} - (F_2)_{ij}| \quad (1)$$

and

$$d_2(y_1, y_2) := d_2(F_1, F_2) = \sqrt{\sum_{i,j} ((F_1)_{ij} - (F_2)_{ij})^2} \quad (2)$$

For ranked genealogies G_1 and $G_2 \in \mathcal{G}_n$, with corresponding F_1 and F_2 , \mathbf{F} -matrices

$$d_1(G_1, G_2) := \sum_{i,j} |(F_1)_{ij}(W_1)_{ij} - (F_2)_{ij}(W_2)_{ij}|,$$

and

$$d_2(G_1, G_2) := \sqrt{\sum_{i,j} ((F_1)_{ij}(W_1)_{ij} - (F_2)_{ij}(W_2)_{ij})^2},$$

where W_1 and W_2 are weight matrices constructed using the respective branching event times $u_k = (u_{k,n}, u_{k,n-1}, \dots, u_{k,1})$ of the k -th tree, $k = 1, 2$ with $(W_k)_{ij} := |u_{k,j} - u_{k,i+1}|$ (Figure 1(B)).

For defining a distance on the space of heterochronous ranked tree shapes or genealogies (Figure 1(C)), Kim et al. [2019] propose supplementing the \mathbf{F} -matrix with additional rows for sampling events. The heterochronous d_1 and d_2 distances are then computed analogously to the isochronous distances, as the L_1 and L_2 distances between the extended \mathbf{F} -matrices of the same size, as detailed in Section 3 of the appendix of Kim et al. [2019]. For improving computational efficiency when computing pairwise distances among a large number of trees, we modify the distance slightly and consider all trees together when adding additional rows to the \mathbf{F} -matrix. Further details can be found in Section A in the appendix.

3 Central summaries

Let $y_1, \dots, y_m \in \mathcal{T}_n$ be m ranked tree shapes with n leaves independently drawn from a common probability distribution. We are interested in summarizing such samples and identifying a representative ranked tree shape of the sample. Similarly, given a probability distribution over the space of ranked tree shapes, we are interested in knowing what is the “expected” tree of that distribution.

In evolutionary biology applications, trees are usually not directly observed. Instead, researchers either find a single tree via maximum likelihood estimation or maximum parsimony [Felsenstein, 2004], or generate a large sample of trees from the posterior distribution via Markov chain Monte Carlo methods [Suchard et al., 2018]. In the latter case of Bayesian inference, it is not clear how to best summarize a sample of ranked unlabelled trees and define a representative “mean” tree as a measure of centrality. A decision theoretic approach is to use the d_1 and the d_2 distance metrics to define the absolute and the squared error loss functions. Minimizing the expected posterior losses gives us the posterior median and posterior mean respectively. However, the value that minimizes the expected posterior loss in Euclidean space does not usually correspond to a tree. In particular for d_2 , the Euclidean mean of the \mathbf{F} -matrices may not even be a matrix of integers. However, we can restrict the minimizer to be an element of the space. The resulting summary is the sample posterior Fréchet mean. Similarly, in applications when a random sample of trees or a population of trees is available, the Fréchet mean would be the tree in the space that minimizes the empirical mean loss and the expected loss respectively.

Current practices for summarizing labelled trees include reporting a majority-rule consensus tree (MRC), a maximum clade credibility (MCC), and a median tree based on metrics on labelled trees [Benner and Bačák, 2013, Brown and Owen, 2019]. The MRC is obtained by choosing partitions with probability greater than 0.5 from the list of observed partitions and it is usually annotated with marginal probabilities of each partition as a measure of uncertainty [Cranston and Rannala, 2007]. The MCC tree is the tree with the maximum product of clade probabilities and it is arguably, the most used central summary of labelled trees.

The concept of consensus partition is not longer applicable for ranked tree shapes. Instead, we rely on the

proposed distances on ranked tree shapes to define the Fréchet mean in the same line as the median tree for labelled trees. The Fréchet mean is the tree in the space that has the minimum expected squared distance to a tree in the space, and hence it provides a natural notion of central tree. We extend the notion to ranked genealogies, including heterochronous genealogies.

3.1 The Fréchet mean

We first consider the metric spaces (\mathcal{T}_n, d) , where d is either d_1 or d_2 , and let μ denote a finite probability mass function on \mathcal{T}_n , then the barycenter of μ , also called a Fréchet mean tree [Fréchet, 1948], is any element $\bar{T} \in \mathcal{T}_n$ such that

$$\bar{T} \in \operatorname{argmin}_{x \in \mathcal{T}_n} \sum_{y \in \mathcal{T}_n} d(x, y)^2 \mu(y). \quad (3)$$

Since \mathcal{T}_n is finite, we immediately have the existence of the minimizer in Equation 3. Note that uniqueness may not be guaranteed, as though the objective function is convex, the space is discrete. If there is more than one minimizer, the elements of the Fréchet mean set will be close to each other in the metric d . However, for many generating tree distributions, we observe that the Fréchet mean is unique and for the rest of the paper we consider as our summary one element of the Fréchet mean set.

Examples of probability distributions on \mathcal{T}_n include the Tajima coalescent (Yule model) [Tajima, 1983, Sainudiin et al., 2015] in which $\mu(T) = \mu(F) = \frac{2^{n-c-1}}{(n-1)!}$, where c is the number of cherries, i.e., the number of internal nodes subtending two leaves. We consider a larger class of probability distributions on ranked tree shapes in Section 5.

Similarly, for the metric spaces (\mathcal{G}_n, d) with d corresponding to d_1 or d_2 on \mathcal{G}_n and ν a probability measure on \mathcal{G}_n such that

$$\int_{\mathcal{G}_n} d(x, y)^2 d\nu(y) < \infty,$$

the Fréchet mean genealogy is any element $\bar{G} \in \mathcal{G}_n$ such that

$$\bar{G} \in \operatorname{argmin}_{G \in \mathcal{G}_n} \int_{H \in \mathcal{G}_n} d(G, H)^2 d\nu(H). \quad (4)$$

In this manuscript, we will consider probability models on isochronous genealogies such that for $G = (F, \mathbf{u})$, $d\nu(G) = \mu(F) \prod_{j=1}^{n-1} f(u_j | u_{j+1}) d(\mathbf{u})$, that is, the tree topology and the branching event times are independent. In evolutionary biology applications, this assumption corresponds to neutral evolution in a closed population [Wakeley, 2008]. In this case, the Fréchet mean becomes:

$$\bar{G} \in \operatorname{argmin}_{G \in \mathcal{G}_n} \sum_{F, H \in \mathcal{F}_n} \int_0^\infty \int_{u_{n-1}}^\infty \cdots \int_{u_2}^\infty d(G, H)^2 \mu(F^H) f(u_{n-1} | u_n) \cdots f(u_1 | u_2) du_1 du_2 \cdots du_{n-1}. \quad (5)$$

A remarkable property of the mean (Eq. 5) under the d_2 distance on genealogies, is that the optimization problem can be separated into two optimization problems, one for finding the tree topology and one for finding the branching event times. The following proposition formalizes this result.

Proposition 2. Let ν be a probability measure on \mathcal{G}_n , the space of isochronous genealogies, such that the tree topology and branching event times are independent under ν . The Fréchet mean $\bar{G}_2 = (F^*, u^*)$ under the d_2 metric can be obtained by separately finding F^* and u^* .

The proof is in the appendix, in Section C.

The empirical Fréchet mean of a given sample y_1, \dots, y_m from the metric space (\mathcal{T}_n, d) is obtained by taking μ in (3) to be the empirical measure. The mean of a sample h_1, \dots, h_m from (\mathcal{G}_n, d) is obtained analogously, where ν in (4) is taken to be the empirical measure, that is

$$\bar{T} \in \operatorname{argmin}_{x \in \mathcal{T}_n} \sum_{j=1}^m d(x, y_j)^2 \quad (6)$$

$$\bar{G} \in \operatorname{argmin}_{g \in \mathcal{G}_n} \sum_{j=1}^m d(g, h_j)^2 \quad (7)$$

The cardinality of the space \mathcal{T}_n is given by the Euler zigzag numbers (OEIS A000111), which grow super-exponentially with n , $|\mathcal{T}|_n \sim 2(2/\pi)^{n+1} \cdot n!$. Finding the Fréchet mean is hence computationally challenging for large n .

For a simpler summary of centrality, we can use an in-sample version of (6), which we call the *restricted Fréchet mean*:

$$\bar{T}_i^{\text{in-sample}} \in \operatorname{argmin}_{x \in \{y_1, \dots, y_m\}} \sum_{j=1}^m d_i(x, y_j)^2 \quad (8)$$

$$\bar{G}_i^{\text{in-sample}} \in \operatorname{argmin}_{g \in \{h_1, \dots, h_m\}} \sum_{j=1}^m d_i(g, h_j)^2 \quad (9)$$

This may be reasonable for spaces with large number of leaves when direct computation of the Fréchet mean is not possible. However, constraining ourselves to stay only within the sample may be undesirable.

3.2 Mixed Integer Programming

In principle, the definition of the Fréchet mean is not sensitive to the choice of metric. However, in the case of the d_1 and d_2 metrics, the Fréchet mean is the minimizer of a convex objective function. In addition, the space of \mathbf{F} -matrices is characterized by a set of linear inequalities (Theorem 1) and hence the problem of finding the Fréchet mean can be framed as a mixed integer programming problem.

Let μ be a probability measure on \mathcal{T}_n , or equivalently on \mathcal{F}_n , then in the case of the d_2 metric, the Fréchet mean \bar{F}_2 is given by:

$$\begin{aligned} \bar{F}_2 &\in \operatorname{argmin}_{F \in \mathcal{F}_n} \sum_{H \in \mathcal{F}_n} \sum_{k,l} (F_{kl} - H_{kl})^2 \mu(H) \\ &= \operatorname{argmin}_{F \in \mathcal{F}_n} \sum_{H \in \mathcal{F}_n} \sum_{k,l} (F_{kl}^2 - 2F_{kl}H_{kl}) \mu(H) \end{aligned}$$

$$= \operatorname{argmin}_{F \in \mathcal{F}_n} \sum_{k,l} \{F_{kl}^2 - 2F_{kl}M_{kl}\}$$

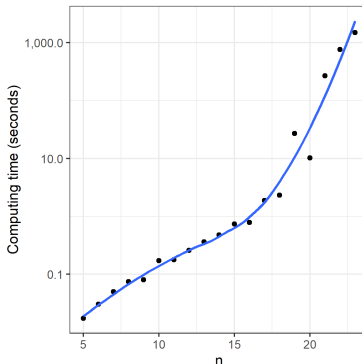


Figure 3: **Running time.** Exact computation for Fréchet mean under the Yule model using Gurobi, plotted against dimension of \mathbf{F} -matrices. Computations done on laptop with an Intel i7 processor.

where $M_{kl} = \sum_{H \in \mathcal{F}_n} H_{kl} \cdot \mu(H)$. This is a simple quadratic objective function with linear and integrality constraints. We use GUROBI [Gurobi Optimization, 2020], a standard MIP solver, to directly perform the optimization. The implementation of the code is available in the R package FMATRIX. Note that once the means M_{kl} are computed, the rest of the problem no longer involves the m samples. That is, the problem scales with the number of leaves n but not with the number of samples m . This is particularly important when summarizing samples obtained through MCMC, since m is usually of high order.

This method works well for small number of leaves n , such as $n = 20$, but it quickly becomes impractical with larger n . Figure 3 shows how the computation time grows exponentially in n . For larger n , we resort to stochastic combinatorial optimization algorithms that scale well at the expense of solution guarantees as discussed in Section 3.3.

3.3 Simulated annealing algorithm

When the number of leaves is large, the MIP solution is computationally demanding and often unfeasible. A simple technique that works well is simulated annealing [Kirkpatrick et al., 1983], which is a general-purpose stochastic algorithm for optimizing an objective function over a potentially large discrete set. Simulated annealing explores the ranked tree shape space via a Metropolis-Hastings algorithm. We trade the guarantee of an exact solution for computational tractability.

In order to describe the simulated annealing algorithm, we define two Markov chains on the space of ranked tree shapes (one for isochronous and one for heterochronous trees) in Section D of the appendix. The two Markov chains are then used as proposal distributions in the Metropolis-Hastings step of the simulated annealing algorithm.

In the case of the Fréchet mean, SA aims to minimize the energy function $E(x) = \sum_{i=1}^m d(x, y_i)^2$ for a sample of trees $\{y_i\}_{i=1}^m$ over $x \in \mathcal{T}_n$. This problem is equivalent to finding the maximum of $\exp\{-E(x)/R\}$

at any given temperature $R > 0$. Let $\{R_k\}$ be a sequence of monotone decreasing temperatures such that $\lim_{k \rightarrow \infty} R_k = 0$, for example $R_k = \alpha^k R_0$ for some high initial temperature R_0 , and $\alpha < 1$. (This is the exponential cooling schedule.) Then, at each temperature, the SA algorithm consists of Metropolis-Hastings (MH) steps that targets $\pi_k(x) \propto \exp\{-E(x)/R_k\}$ as the stationary distribution. As the number of steps increases, $\pi_k(x)$ puts more and more of its probability mass in the set of global maxima. SA differs from descent algorithms by allowing transitions to higher energy states at higher temperatures, in order to avoid being stuck at local maxima.

In our implementations (Algorithm 1) for isochronous and heterochronous Fréchet means, the MH proposal distributions are given by the transition kernels of the Markov chains described in section D of the appendix. In both cases, the transition kernels are symmetric and hence, the MH acceptance probability of moving from x_{k-1} to x_k is given by:

$$a_k = \exp\left(-\frac{E(x_k)}{R_k} + \frac{E(x_{k-1})}{R_{k-1}}\right) \wedge 1.$$

The temperature schedule in SA needs to be specified and affects the time taken for convergence of the algorithm. Theoretical convergence guarantees exist for the logarithmic cooling schedule $R_k = R_0(1 + \alpha \log(1 + k))^{-1}$ with sufficiently high initial temperature and appropriately chosen α (see Chapter 3 of Aarts and Korst [1988]). However this schedule is prohibitively slow for most problems. In practice, we observe that the exponential cooling schedule with α chosen very close to 1 performs reasonably well. The benefits of simulated annealing are its easy implementation and the design of the algorithm which allows getting out of local optima.

Algorithm 1 Fréchet mean of a sample of ranked unlabelled trees via simulated annealing

Require: T_1, \dots, T_m sample of ranked unlabelled trees, starting position $T^{(0)}$, initial temperature $R_0 > 0$, decay parameter $\alpha \in (0, 1)$.

Define energy function $E(T) = \sum_{i=1}^m d(T, T_i)^2$. (d is a metric defined in Section 2)

$k \leftarrow 0$

repeat

$S \leftarrow$ random neighbour of $T^{(k)}$ (*generate proposal using Markov chains of Definitions 11 or 14, for isochronous and heterochronous trees respectively*)

if $\text{runif}(1) < \exp\left(-\frac{E(S) - E(T^{(k)})}{R_k}\right)$ **then**

$T^{(k+1)} \leftarrow S$ (*accept*)

else

$T^{(k+1)} \leftarrow T^{(k)}$ (*reject*)

end if

$R_{k+1} \leftarrow \alpha R_k$ (*reduce temperature*)

$k \leftarrow k + 1$

until convergence of $T^{(k)}$

Using the result shown in Section 3.2, we can replace the energy function $E(T) = \sum_{i=1}^m d(T, T_i)^2$ in the case of the d^2 metric by $E(T) = \|F - M\|^2$ where F is the \mathbf{F} -matrix corresponding to T and M is the Euclidean mean of the \mathbf{F} -matrices corresponding to the T_i .

We note that for both isochronous and heterochronous genealogies, our algorithm first finds the average coalescent times and then finds the tree topology via the SA algorithm just described. In the case of heterochronous genealogies, the Markov chain used is conditioned on a fix set of coalescent and sampling times. We analyse the computational performance of the SA algorithm in the appendix.

4 Measures of dispersion

In this section we define and discuss three notions for quantifying uncertainty or dispersion in a distribution or a sample of ranked tree shapes (or ranked genealogies).

The **Fréchet variance** is a natural measure of dispersion for arbitrary probability metric spaces. It measures the concentration around the Fréchet mean. While the Fréchet mean is an object of the metric space, the Fréchet variance is a simple scalar summary of spread.

Let μ be a probability measure on \mathcal{T}_n (\mathcal{F}_n). The *Fréchet variance* of $y \sim \mu$ with respect to the metric d is defined as follows:

$$V = \sum_{y \in \mathcal{T}_n} d(y, \bar{T})^2 \cdot \mu(y), \quad \text{where} \quad \bar{T} = \operatorname{argmin}_{x \in \mathcal{T}_n} \sum_{y \in \mathcal{T}_n} d(x, y)^2 \cdot \mu(y) \quad (10)$$

Let $y_1, \dots, y_m \in \mathcal{T}_n$ be a random sample of ranked tree shapes. Then the *sample Fréchet variance* is given by

$$V_m = \frac{1}{m} \sum_{i=1}^m d(y_i, \bar{T})^2, \quad \text{where} \quad \bar{T} = \operatorname{argmin}_{x \in \mathcal{T}_n} \sum_{i=1}^m d(x, y_i)^2 \quad (11)$$

Similarly, the Fréchet variance of $G \sim d\nu$ can be obtained by integrating over the probability space of branching event times and ranked tree shapes.

Another scalar measure of dispersion is **entropy** [Mezard and Montanari, 2009]. Entropy is a function of the probability measure only and it does not depend on the metric d . A measure with zero entropy is concentrated on a single point, and a large entropy indicates greater uncertainty in the position of a random variable with the underlying measure.

Let μ be a probability measure on \mathcal{T}_n . The *entropy* of the space is given by

$$H = - \sum_{y \in \mathcal{T}_n} \mu(y) \cdot \log [\mu(y)] \quad (12)$$

The discrete distribution with maximum entropy is the uniform distribution. While entropy is meaningful at the population level, it does not provide a meaningful value for a given sample. In Figure 5 we compare entropy with Fréchet variance for a particular class of probability models on ranked tree shapes.

In many applications, a single mean value and the variance are not enough for summarizing the distribution. **Interquartiles and credible intervals** are typically used to inform about the concentration of the

For example $T^{(\text{unb})} \preceq_{\text{lex}} T^{(\text{bal})}$ and $T^{(\text{unb})} \preceq_{\text{lex}} T \preceq_{\text{lex}} T^{(\text{bal})}$ for any $T \in \mathcal{T}_n$. Although the lexicographic order is a total order, we propose to order all ranked tree shapes in the space according to their signed distance to T_K and to only use the lexicographic order within equivalence classes as follows.

Definition 6. We say that $T_1 \preceq T_2$ if $f(T_1) < f(T_2)$ or if $f(T_1) = f(T_2)$ and $T_1 \preceq_{\text{lex}} T_2$.

Proposition 7. The order induced by \preceq of Definition 6 on \mathcal{T}_n is a total order.

Proof. To show antisymmetry note that the only way $T_1 \preceq T_2$ and $T_2 \preceq T_1$ is that $f(T_1) = f(T_2)$ and $T_1 \preceq_{\text{lex}} T_2$ and $T_1 \succeq_{\text{lex}} T_2$. This occurs only if $F^{(1)} = F^{(2)}$. The bijection of Theorem 1 then implies that $T_1 = T_2$. Transitivity and convexity follow directly from the transitivity and convexity of $<$ and \preceq_{lex} . \square

We note that \preceq_{lex} is not the only possible lexicographic order; for example a row-vectorized representation of $T \in \mathcal{T}_n$ can be replaced in definition 5 to generate another ordering. Although the lexicographic order is not a biologically meaningful order, it provides a consistent way for comparing histograms across different tree models on the same space (see for example, the third row of Figure 6).

Having established the \preceq order, we will summarize credible balls and interquartile balls by at most four ranked tree shapes and by at least two ranked tree shapes. Let $B_\varepsilon(\bar{T})$ denote the interquartile or credible ball and \bar{T} the Fréchet mean of the distribution. Then the set of ranked tree shapes at the boundary of $B_\varepsilon(\bar{T})$ will be partitioned into two sets, one with positive signed distance to \bar{T} and one with negative signed distance to \bar{T} . If the cardinality of the sets is greater than one, we will then summarize each set by the smallest and the largest ranked tree shape in each set according to the \preceq order.

5 Results

5.1 Statistical summaries of Blum-François distributions on ranked tree shapes

We present and analyse point summaries of a large family of ranked tree shape models called the Blum-François β -splitting model. After the introduction of Aldous' β -splitting model on cladograms (tree shapes without rankings) [Aldous, 1996, 2001], many extensions and generalizations of this model have been proposed on different resolutions of trees, including the Blum-François model on ranked tree shapes [Sainudiin and Véber, 2016] and the alpha-beta splitting model [Maliot et al., 2018]. Henceforth, we will refer to the Blum-François model on ranked tree shapes simply as the **Blum-François model**.

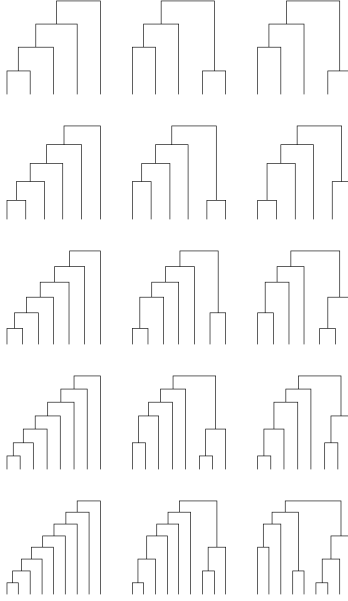


Figure 4: **Fréchet mean under the Blum-François β -splitting model.** Top to bottom: $n = 5, \dots, 9$, Left to right: $\beta = -1, 0, 100$.

We start with the Blum-François model on ranked unlabelled *planar* trees (there is distinction between left and right offspring). Let n_i^L and n_i^R denote the number of internal nodes in the left and right subtrees below node i . In particular, if node i is a cherry, i.e. subtends two leaves, then $n_i^L = n_i^R = 0$. Then, a ranked unlabelled planar tree with n leaves has probability mass function given by:

$$P(T_{\text{planar}}) = \prod_{i=1}^{n-1} \frac{B(n_i^L + \beta + 1, n_i^R + \beta + 1)}{B(\beta + 1, \beta + 1)}$$

where $B(a, b) = \int_0^1 x^{a-1}(1-x)^{b-1} dx$ is the Beta function and $\beta \in [-1, \infty)$. A ranked tree shape T obtained by ignoring the distinction between left and right subtrees has then the following probability mass function:

$$P(T) = 2^{n-1-c} \prod_{i=1}^{n-1} \frac{B(n_i^L + \beta + 1, n_i^R + \beta + 1)}{B(\beta + 1, \beta + 1)}$$

where c is the number of cherries in T . The β parameter controls the level of balancedness of the distribution. In particular, when $\beta = 0$, the corresponding distribution $P(T) = 2^{n-1-c}/(n-1)!$ is the coalescent distribution on ranked tree shapes (Kingman coalescent), also known as the Yule distribution.

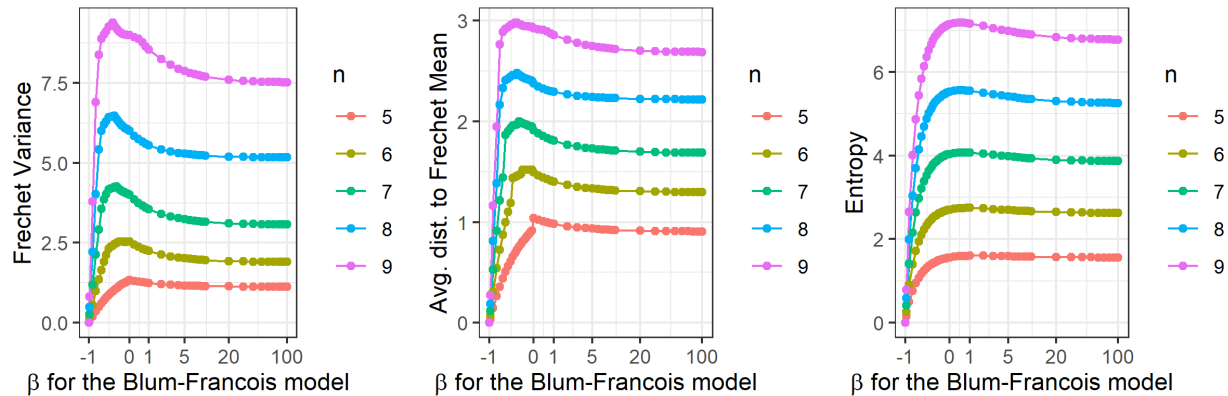


Figure 5: **Measures of dispersion.** Fréchet variance, average distance to Fréchet mean, and entropy, for small n under the Blum-François β -splitting model

Figure 4 shows the d_2 Fréchet means of the ranked tree shapes distributions with $5, \dots, 9$ leaves under the Blum-François distribution with $\beta \in \{-1, 0, 100\}$. For small values of β , the distribution generates unbalanced trees and for large values of β , the distribution generates balanced trees. Figure 5 shows the d_2 Fréchet variance, expected distance to the Fréchet mean and entropy for $n = 5, \dots, 9$ and β values spaced out in $[-1, \infty]$. For $\beta > 1$, the variance and entropy remain relatively constant as functions of β . The largest variance and entropy are obtained when $\beta \leq 0$. We explicitly compute the corresponding Fréchet mean, Fréchet variance, and entropy for small n by enumerating all the ranked tree shapes and evaluating their probability mass functions.

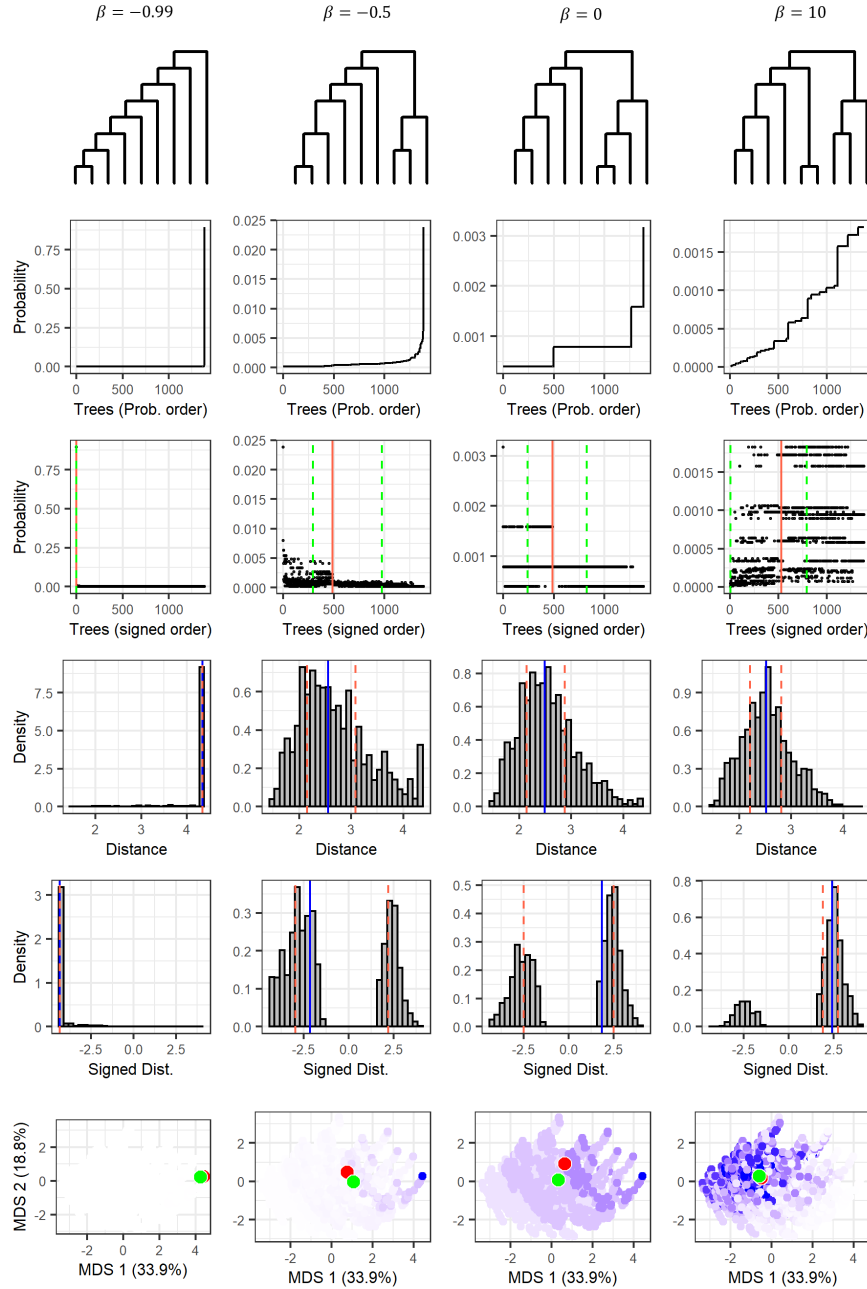


Figure 6: **Summarizing Blum-François distributions on ranked tree shapes.** Blum-François distributions on ranked tree shapes with $n = 9$ leaves, columns correspond to $\beta = -0.99, -0.5, 0$ (coalescent), 10 respectively. Row 1: Fréchet Mean of the distribution; Row 2: Probability mass function of trees, arranged in increasing order of probability; Row 3: Probability mass function of trees, arranged in the Signed Distance order of Definition 6, with Fréchet mean (red line) of distribution and interquartiles (green dashed lines); Row 4: Histogram of distance to the Kingman Fréchet mean, with median (blue line) and interquartiles (orange dashed lines) of the distance to the mean; Row 5: Histogram of signed distance to the Kingman Fréchet mean, with median (blue line) and interquartiles (orange dashed lines) of the signed distance; Row 6: Multidimensional scaling visualization of the tree distribution, each dot represents a tree colored by its probability mass, with Fréchet mean (red dot) and expected value (green dot).

For ranked tree distributions with $n = 100$ leaves, we simulated $N = 1000$ ranked tree shapes with the R package `APTREESHape` [Maliet et al., 2018] and found the d_2 mean via the simulated annealing of Section 3.3. The resulting means are shown in Figure 7 for $\beta \in \{-1.9, -1.5, -1, 0, 100\}$.

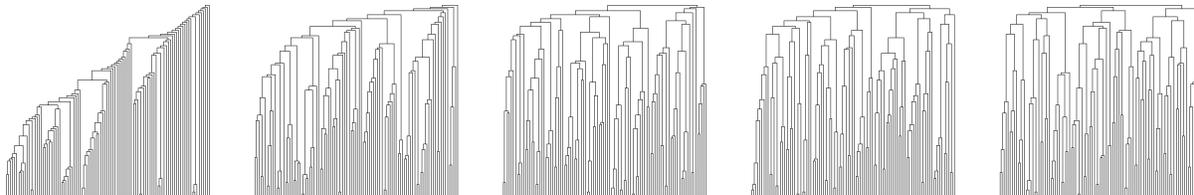


Figure 7: **Approximated Fréchet means.** Fréchet means are found via simulated annealing from a sample of $N = 1000$ trees with $n = 100$ leaves from β -splitting distribution. Left to right: $\beta = -1.9, -1.5, -1, 0, 100$. Simulated annealing with exponential cooling schedule and decay parameter .9995, initial temperature 1000.

Figure 6 shows different summaries of four Blum-François distributions on ranked tree shapes with $n = 9$ leaves. The second row correspond to the probability mass function with trees (x-axis) arranged in increasing order of probability. When analyzing these plots, it is impossible to assess whether the $\beta = -0.5$ distribution puts more probability mass on unbalanced trees than balanced trees when compared to the $\beta = 10$ distribution since the x-axes are not comparable. The third row shows the probability mass functions with the x-axes arranging trees in the signed distance total order. Here, all x-axes correspond to the same tree arrangements. It is now clear that the $\beta = -0.5$ distribution assigns more probability mass to unbalanced trees and the $\beta = 10$ distribution assigns more mass to balanced trees. This is confirmed in the fifth row of Figure 6. The histogram of the signed distance to the mean is skewed to the right (balanced) when $\beta = 10$.

Row four of Figure 6 shows the histograms of the distance to the mean. This one-dimensional summary of the tree distributions hinders whether some distributions put more probability mass to different types of trees. For example the last three histograms of the fourth column look very similar. Finally, while the MDS plots (Figure 6, last row) only explain about 53% of all pairwise distances, the last panel shows the distinctions between the four probability mass distributions. Here, green dots corresponds to the points whose \mathbf{F} -matrix is $\mathbb{E}(F)$ (and do not lie in tree space) and red dots are the Fréchet means.

We note that the Fréchet means of the distributions with $\beta = 0.05, 0$ and 10 are very close to each other. This indicates that a single central summary may not have a good discriminating power for detecting difference in distributions within the Blum-François family.

5.2 Characterization of mean Kingman tree

As stated in Section 3.2, under d_2 , the population Fréchet mean is given by

$$\bar{F}_2 = \operatorname{argmin}_{F \in \mathcal{F}_n} \sum_{k,l} \{F_{kl}^2 - 2F_{kl}M_{kl}\},$$

where $M_{kl} = \mathbb{E}(F_{k,l})$. If we know the matrix M , we only need to search for ranked tree shapes that are in a neighborhood of M (see for example the red and green dots representing the M and the Fréchet mean in the last row of Figure 6). In fact, the only data input needed using GUROBI or simulated annealing is M . Although there is no explicit formula for the Fréchet mean for the distributions analyzed here, there is an explicit formula for M for the Kingman/Yule coalescent distribution (Blum-François with $\beta = 0$). In Figure 6, we visualize M and the Fréchet mean in an MDS plot of the entire space.

Theorem 8. Let $F \in \mathcal{F}_n$ be an \mathbf{F} -matrix distributed according to the Blum-François model with $\beta = 0$, i.e. according to the Kingman/Yule coalescent distribution, then:

1. The distribution of the i -th row of F is independent of n .

2. $\mathbb{E}[F_{i,j}] = \frac{j(j+1)}{i}$

3. $\text{Var}[F_{i,j}] = \frac{j^3 2(j+1)^2}{i^2(i-1)} + \frac{j(j+1)(i-2j-1)}{i(i-1)}$

4. $\text{Cov}[F_{i_1 j_1}, F_{i_2 j_2}] =$

$$\begin{cases} \frac{j_1(j_1+1)[j_2(j_2+2)+(i_1+1)(i_1-2j_2-2)]}{i_1^2(i_1-1)} & \text{when } i_1 = i_2, j_1 < j_2 \\ \frac{j_2(j_2+1)(j_2-i_2)(j_2-i_2+1)}{i_1 i_2 (i_2-1)} & \text{when } i_1 > i_2, j_1 = j_2 \\ \frac{j_2(j_2+1)[(j_1+1)(j_1+2)+(i_1+1)(i_1-2j_1-2)]}{i_1^2(i_1-1)} + \frac{(i_1-i_2)j_1 j_2 (j_2+1)}{i_1 i_2} \begin{bmatrix} \frac{j_1-1}{i_2-1} & -\frac{j_1+1}{i_2+1} \end{bmatrix} & \text{when } i_1 > i_2, j_1 > j_2 \\ \frac{j_1(j_1+1)[(j_2+1)(j_2+2)+(i_1+1)(i_1-2j_2-2)]}{i_1^2(i_1-1)} + \frac{(i_1-i_2)j_1(j_1+1)j_2}{i_1 i_2} \begin{bmatrix} \frac{j_2-1}{i_2-1} & -\frac{j_2+1}{i_2+1} \end{bmatrix} & \text{when } i_1 > i_2, j_1 < j_2 \end{cases}$$

The proof can be found in Section E in the appendix.

The relevance of Theorem 8 is that for one of the most popular models in population genetics: the coalescent [Wakeley, 2008], the Fréchet mean can be obtained for any n , without the need for simulating a sample from the distribution as it is done in Figure 7. Moreover, given a sample of \mathbf{F} -matrices, the sample average (element-wise) converges almost surely to M by the law of large numbers. Theorem 8 together with the Multivariate Central Limit Theorem [Hogg et al., 2019, Thm 5.4.4], could be used to test whether a random sample of ranked tree shapes follows the standard coalescent distribution such as the Kingman/Yule model.

Theorem 9. (Central Limit Theorem for \mathbf{F} -matrices) Let $F^1, \dots, F^m \in \mathcal{F}_n$ be an i.i.d. sample of \mathbf{F} -matrices drawn from some distribution P . Let $\bar{F}_m \in \mathbb{R}^{(n-1) \times (n-1)}$ be the matrix whose entries correspond to the sample average of F^1, \dots, F^m (entrywise). Then

$$\sqrt{m}(\bar{F}_m - M) \xrightarrow{d} N(\mathbf{0}, \Sigma) \tag{16}$$

where the mean $M \in \mathbb{R}^{(n-1)^2}$ is given by

$$\mu_{ij} = \mathbb{E}_P[F_{ij}]$$

and the covariance tensor $\Sigma \in \mathbb{R}^{(n-1)^2 \times (n-1)^2}$ is given by

$$\Sigma_{ij,kl} = \text{Cov}_P[F_{ij}, F_{kl}]$$

Proof. The proof follows directly from the multivariate central limit theorem, considering the \mathbf{F} -matrices as elements of $\mathbb{R}^{(n-1)^2}$. Since each entry of the \mathbf{F} -matrices is bounded in $[0, n]$, all expectations are finite. \square

Corollary 9.1. Consider the setting of Theorem 9, and assume that Σ is invertible. Let $\hat{\Sigma} \in \mathbb{R}^{(n-1)^2 \times (n-1)^2}$ be the empirical covariance tensor. We have

$$\hat{\Sigma}^{-1/2} \sqrt{m} (\bar{F}_m - \mu) \xrightarrow{d} N(\mathbf{0}, \mathbf{I}) \quad (17)$$

where $\mathbf{I} \in \mathbb{R}^{(n-1)^2 \times (n-1)^2}$ is the identity tensor given by

$$\mathbf{I}_{ij,kl} = \mathbf{1}_{i=k, j=l}$$

Proof. The proof follows by the multivariate version of Slutsky's theorem, using consistency of the empirical covariance, and the fact that the function $M \rightarrow M^{-1/2}$ is continuous when M is an invertible covariance matrix. \square

5.3 Summaries of coalescent ranked genealogical distributions

In neutral (isochronous) coalescent models with variable population size, the tree topology and the distribution of branching event waiting times are independent. The ranked tree shape is distributed according to the Kingman/Yule/Blum-François model with $\beta = 0$ and the branching event times have the following conditional density:

$$f(u_{i-1} | u_i, N_e(t)) = \frac{\binom{i}{2}}{N_e(u_{i-1})} \exp \left\{ - \binom{i}{2} \int_{u_i}^{u_{i-1}} \frac{du}{N_e(u)} \right\}, \quad (18)$$

with $u_n = 0$ and $N_e(t)$ is a non-negative function that denotes the effective population size [Slatkin and Hudson, 1991].

We simulated 1000 ranked genealogies according to the neutral coalescent model with the following effective population size functions:

- (1) Constant: $N_e(t) = 10000$;
- (2) Exponential: $N_e(t) = 10000 \exp\{-0.01t\}$;
- (3) Logistic:

$$N_e(t) = \begin{cases} 1000 + \frac{9000}{1 + \exp[6 - 2(t \bmod 12)]} & (t \bmod 12) \leq 6 \\ 1000 + \frac{9000}{1 + \exp[-18 + 2(t \bmod 12)]} & (t \bmod 12) > 6. \end{cases}$$

Figure 8 shows the Multidimensional scaling representation of the three simulated distributions (using d_2), together with the Fréchet means (stars) and medois (triangles). The corresponding means and triangles are depicted in Figure 9. Fréchet mean topologies are calculated with simulated annealing and the branching event times correspond to the sample means. Although in this case the two summaries (means and medois)

are close to each other in MDS, the two genealogies can have very different branch lengths as in the logistic simulation (last row, Figure 9).

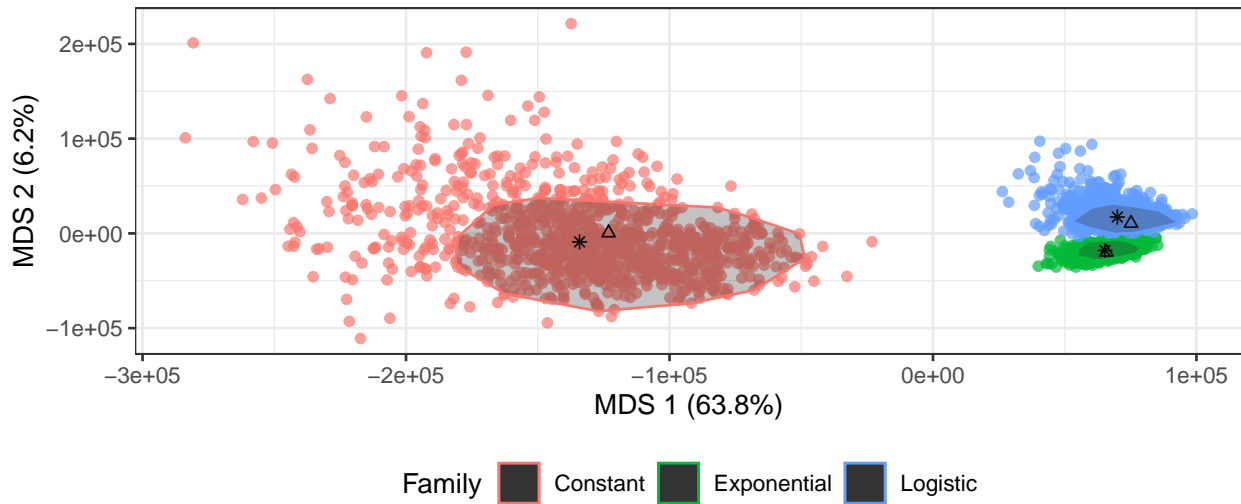


Figure 8: **MDS of ranked genealogies with different branching event times distributions.** Multi-dimensional scaling visualization of the coalescent distributions on ranked genealogies with varying effective population sizes: constant (red), exponential (green), and logistic (blue). Triangles denote medoids and stars denote Freéchet means. Shaded areas represent the 50% convex hulls.

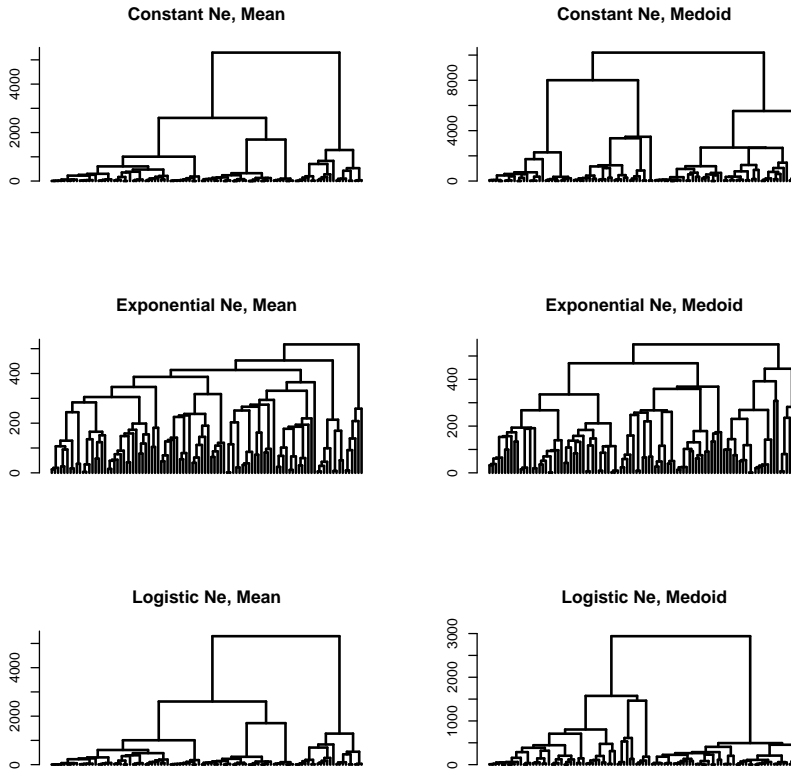


Figure 9: **Fréchet mean vs medoid.** Fréchet means (first column) and in-sample medoids (second column) of the three simulated coalescent distributions of genealogies with $n = 100$ leaves and with varying effective population size trajectories. Fréchet means are indicated as stars and in-sample medoids as triangles in Figure 8. Fréchet means coalescent times are the sample mean coalescent times.

6 Analysis of SARS-CoV-2

The COVID-19 pandemic has had an enormous impact on all humanity. Tracking the evolution of the SARS-CoV-2 virus that causes COVID-19 has been of great importance for tracking the epidemic and for improving our understanding of the disease [Volz et al., 2021]. Here we analyse SARS-CoV-2 molecular sequences publicly available in the GISAID EpiCov database [Shu and McCauley, 2017] from the states of California, Florida, Texas and Washington in the USA for the period of February 2020 to September 2020.

A great challenge in molecular epidemiology of SARS-CoV-2 consists in being able to analyse all available sequences from a population. The number of available sequences exceeds the sample capacity that any Bayesian phylogenetic method (for example those implemented in BEAST [Suchard et al., 2018]) can handle. The predominant approach is to subsample the available sequences and infer the posterior genealogical distribution with BEAST. One important question then is how to assess whether the chosen sample’s estimated genealogy is representative to the mean genealogy in the population of a sample of the same size

as our subsample. Here, we compare subposterior distributions estimated from different random samples of 100 sequences from California and assess the stability of their Fréchet means.

We selected 9 samples of 100 sequences uniformly at random, obtained in California before June 1 of 2020 and 9 random samples of 100 sequences obtained after June 1, 2020. For each study (random set of 100 samples), we generated 1,000 MCMC samples thinned every 50,000 iterations from the posterior distribution of model parameters (genealogy and other parameters) with BEAST [Suchard et al., 2018]. Details of parameters and prior distributions selected for BEAST analyses and data access acknowledgments can be found in the appendix.

We first analyse the California trees sampled from a single posterior distribution. For ease of visualization, we show the MDS plot of all 1000 posterior genealogical samples in Figure 10 assuming the d_2 metric defined in Definition 2. The posterior central genealogies are depicted as colored dots in Figure 10 and the corresponding genealogies are drawn in Figure 11. The two tree topologies of the Fréchet means are obtained with our simulated annealing algorithm for heterochronous samples. The Fréchet mean coalescent times are obtained as sample averages (purple tree in Figure 10) and sample medians (cyan tree in Figure 10). Note that the two tree topologies of the Fréchet means are different. As mentioned in section 3.3, our SA algorithm finds the tree topology that optimizes the objective function conditioned on a given sequence of sampling and coalescing events. The maximum clade credibility (MCC) tree is computed using the R package PHANGORN. We also plot the in-sample medoid, which is the tree in the sample that minimizes the average distance to the rest of the trees in the sample. We shaded the 50% credible convex hull around the Fréchet mean with mean coalescent times. All central summaries are within the 50% credible convex hull.

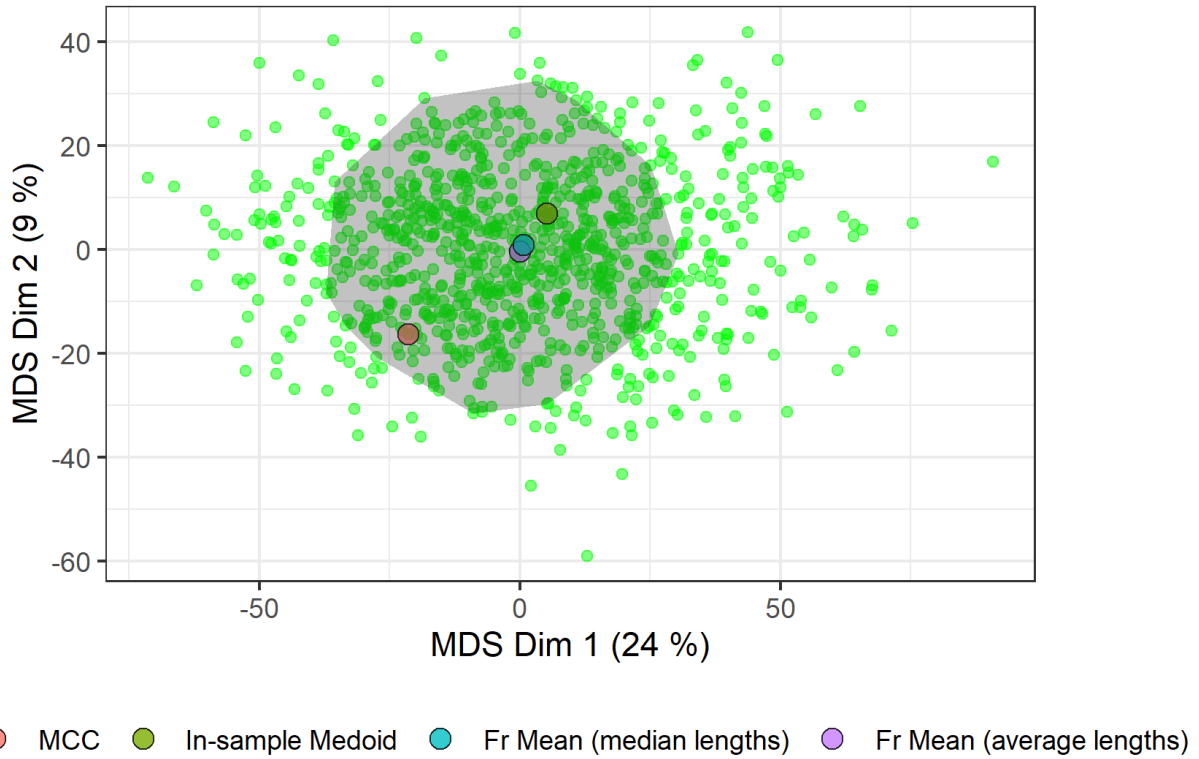


Figure 10: **MDS plot of a sample of $N = 1000$ trees from a single BEAST posterior distribution of California.** Each dot represents a tree of $n = 100$ sequences randomly chosen among GISAID sequences from California sequenced between February and May 2020. Shaded area corresponds to 50% credible convex hull around the Fréchet mean, using average branch lengths.

Remark: We note that both the Fréchet mean and the in-sample medoid are designed to be central with respect to the d_2 metric using F-matrices, whereas the MCC tree is not. Hence, it is not surprising that the MCC tree is further away from the center in the MCC plot as compared to the other point summaries. We can notice that both Fréchet means are closer to the center than the in-sample medoid.

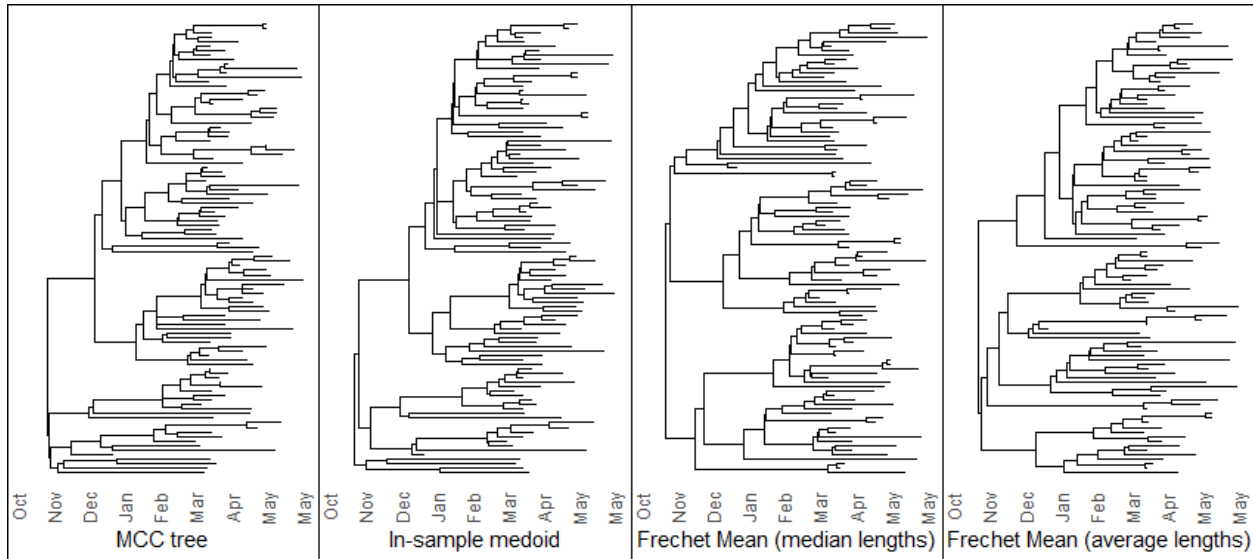


Figure 11: **Posterior summary trees of a sample of 100 sequences from California Feb-May 2020** Summary trees for a sample of 1000 trees drawn from a single BEAST posterior using $n = 100$ sequences from California. Left to right: Maximum Clade Credibility tree obtained with PHANGORN, in-sample medoid, Fréchet mean using median coalescent times, and Fréchet mean using average coalescent times. The four trees correspond to the four dots highlighted in Figure 10.

We now visualize multiple subposterior distributions of California together in the MDS plot of Figure 12 using the d_2 metric. For ease of visualization we further subsampled only 20 trees (evenly spaced) from each BEAST posterior distribution to generate the MDS plot. The first group of trees on the left correspond to trees of samples sequenced between February and May 2020, and the second group on the right correspond to trees of samples sequenced between Jun-Sep 2020. The Fréchet means are then computed with the SA algorithm for each subsample (shown as bigger dots with black border). As expected, the separation between samples from different time periods may reflect the fact that California experienced an increase in COVID-19 prevalence in the second semester of 2020. Moreover, samples from the second time period are more spread. The separation between the Fréchet means of the two groups suggests that they could be good statistics in a two-sample (or k -sample) test for equality of distributions. We note that even for the first period, some subposterior distributions in California do not overlap.

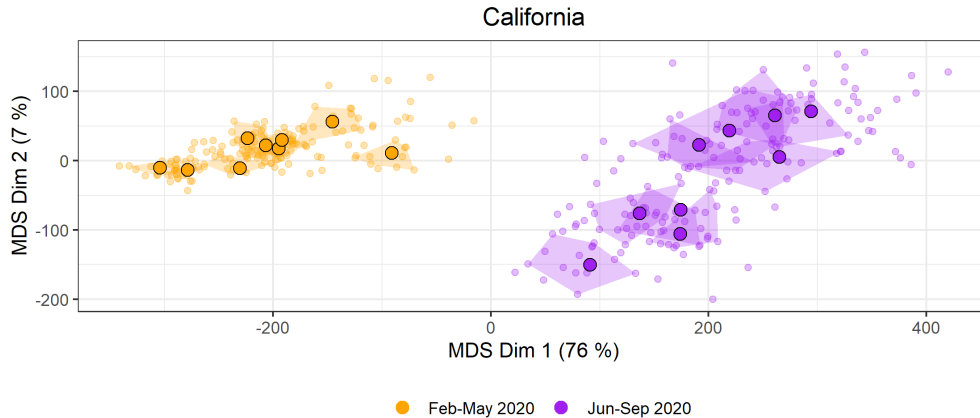


Figure 12: **MDS plot of 20 trees per each of the 18 posterior BEAST samples of trees with $n = 100$ leaves of California.** The group of trees on the left correspond to trees of samples sequenced Feb-May 2020 and the second group of trees on the right correspond to trees of samples sequenced between Jun-Sep 2020. The Fréchet means are calculated using the average coalescent times and are marked as red dots.

We now compare posterior distributions across the four states: California, Washington, Texas and Florida. Figure 13 shows the MDS plot of three samples of 20 trees with $n = 100$ leaves from each location. Sequences analyzed were genotyped between February and May 2020. After computing the Fréchet means, we downsample in order to better visualize the multidimensional scaling plot. We note that the subposteriors of Washington state are more concentrated than any of the other 3 states. Moreover, there is almost no overlap between the posterior genealogical distribution of Washington state with the posterior distributions of the other states. Indeed the reported number of confirmed COVID-19 cases in Washington state is the lowest and with smallest growth rate of all the states considered in this analysis (Figure 14). We note that in the case of Washington state we observe stable subposteriors; all subposteriors reflect the same evolutionary signal.

The posterior distributions of Florida are the second more concentrated in that their three Fréchet means are close to each other and their convex hulls overlap. While the posterior distribution of evolutionary trees of Florida are different to those in Washington state, there is some overlap with the posteriors of California and Texas. California experienced the highest cumulative number of cases (Figure 14) and it also has the largest heterogeneity in subposterior distributions. Analyses on different subsamples in California can provide very different results. This large heterogeneity may be the result of local outbreaks sequencing efforts in the area.

Finally, while the cumulative number of reported cases in Texas is not as large as the one reported in California. Texas's subposteriors show similar heterogeneity to California, with similar posterior distributions of evolutionary histories (genealogies).

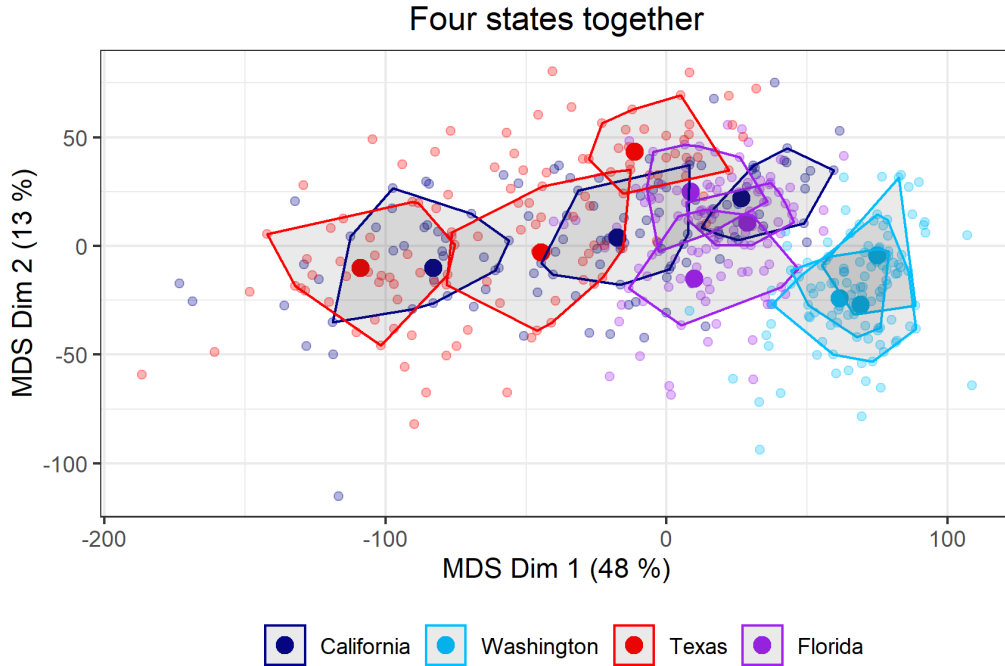


Figure 13: **MDS plot of multiple samples from California, Washington, Florida, and Texas.** Three samples of 20 trees of $n = 100$ samples randomly chosen among GISAID sequences in Feb-May 2020 per location. The Fréchet means are calculated using average coalescent times and marked as red dots. The shaded region corresponds to 50% credible convex hulls around the Fréchet means.

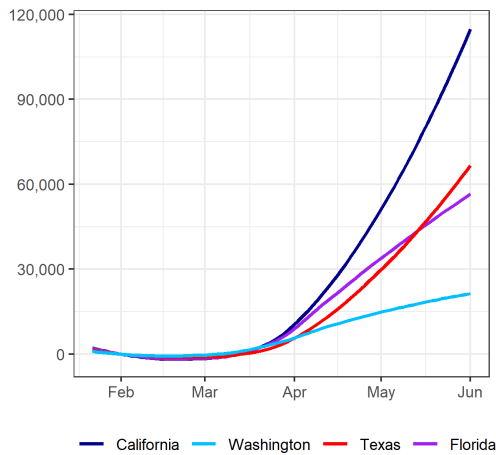


Figure 14: **Confirmed cumulative case counts in California, Washington, Florida, and Texas.** Data between January and September 2020, obtained from the COVID-19 Data Repository by the Center for Systems Science and Engineering (CSSE) at Johns Hopkins University [Dong et al., 2020].

7 Discussion

For discrete tree topologies, the Fréchet mean ranked tree shape may not be unique. However in our experience, we found the Fréchet means to be very close to each other. We conjecture that the set of Fréchet means has a very small diameter and it will be explored in future research. While the non-uniqueness of the Fréchet mean can potentially be problematic for hypotheses testing, we remark that the expected F matrix, here denoted by M , is unique and the limit of the sample mean \bar{F}_m by the strong law of large numbers. In this manuscript, we provided a Central Limit Theorem result for \bar{F}_m and analytical expressions for M and variance of the ranked tree shape distribution under the standard Kingman coalescent. Theoretical results of this kind for other distributions is left as future work. Similarly, analyses of several test statistics based on the distances analyzed here and Fréchet means such as in Dubey and Müller [2019] are subject of future research.

Extension of current work include defining distances and summaries for multifurcating tree shapes and phylogenetic networks. Our current implementations are publicly available in github.com/RSmayak/fmatrix.

Acknowledgement

We acknowledge Paromita Dubey and Jaehee Kim for useful discussions. J.A.P. is supported by National Institutes of Health Grant R01-GM-131404 and the Alfred P. Sloan Foundation.

References

- E. Aarts and J. Korst. Simulated annealing and boltzmann machines. 1988.
- D. Aldous. Probability distributions on cladograms. In D. Aldous and R. Pemantle, editors, Random Discrete Structures, pages 1–18, New York, NY, 1996. Springer New York. ISBN 978-1-4612-0719-1. URL https://doi.org/10.1007/978-1-4612-0719-1_1.
- D. J. Aldous. Stochastic models and descriptive statistics for phylogenetic trees, from yule to today. Statistical Science, 16(1):23–34, 2001. ISSN 08834237. URL <http://www.jstor.org/stable/2676778>.
- P. Benner and M. Bačák. Computing the posterior expectation of phylogenetic trees. 2013.
- L. J. Billera, S. P. Holmes, and K. Vogtmann. Geometry of the space of phylogenetic trees. Advances in Applied Mathematics, 27(4):733 – 767, 2001. ISSN 0196-8858. doi: <https://doi.org/10.1006/aama.2001.0759>. URL <http://www.sciencedirect.com/science/article/pii/S0196885801907596>.
- L. Breiman. Algorithm cart. Classification and Regression Trees. California Wadsworth International Group, Belmont, California, 1984.
- D. G. Brown and M. Owen. Mean and Variance of Phylogenetic Trees. Systematic Biology, 06 2019.
- L. Cappello, A. Veber, and J. A. Palacios. The tajima heterochronous n-coalescent: inference from heterochronously sampled molecular data. arXiv preprint arXiv:2004.06826, 2020.

- J. Chakerian and S. Holmes. Computational tools for evaluating phylogenetic and hierarchical clustering trees. Journal of Computational and Graphical Statistics, 21(3):581–599, 2012.
- K. A. Cranston and B. Rannala. Summarizing a posterior distribution of trees using agreement subtrees. Systematic biology, 56(4):578–590, 2007.
- R. Donaghey. Alternating permutations and binary increasing trees. Journal of Combinatorial Theory, Series A, 18(2):141–148, 1975.
- E. Dong, H. Du, and L. Gardner. An interactive web-based dashboard to track covid-19 in real time. The Lancet infectious diseases, 20(5):533–534, 2020.
- P. Dubey and H.-G. Müller. Fréchet analysis of variance for random objects. Biometrika, 106(4):803–821, 10 2019. ISSN 0006-3444. doi: 10.1093/biomet/asz052. URL <https://doi.org/10.1093/biomet/asz052>.
- B. Efron, E. Halloran, and S. Holmes. Bootstrap confidence levels for phylogenetic trees. Proceedings of the National Academy of Sciences, 93(23):13429–13429, 1996.
- J. Felsenstein. Confidence limits on phylogenies: an approach using the bootstrap. evolution, 39(4):783–791, 1985.
- J. Felsenstein. Inferring phylogenies, volume 2. Sinauer associates Sunderland, MA, 2004.
- M. Fréchet. Les éléments aléatoires de nature quelconque dans un espace distancié. In Annales de l’institut Henri Poincaré, volume 10, pages 215–310, 1948.
- K. Govek, C. Sikes, and L. Oesper. A consensus approach to infer tumor evolutionary histories. In Proceedings of the 2018 Acm international conference on bioinformatics, computational biology, and health informatics, pages 63–72, 2018.
- L. Gurobi Optimization. Gurobi optimizer reference manual, 2020. URL <http://www.gurobi.com>.
- J. Heled and R. R. Bouckaert. Looking for trees in the forest: summary tree from posterior samples. BMC evolutionary biology, 13(1):221, 2013.
- D. M. Hillis, T. A. Heath, and K. S. John. Analysis and visualization of tree space. Systematic biology, 54(3):471–482, 2005.
- R. V. Hogg, J. McKean, and A. T. Craig. Introduction to mathematical statistics. Pearson Education, 2019.
- S. Janson, G. Kersting, et al. On the total external length of the kingman coalescent. Electronic Journal of Probability, 16:2203–2218, 2011.
- M. D. Karcher, J. A. Palacios, S. Lan, and V. N. Minin. phylodyn: an r package for phylodynamic simulation and inference. Molecular ecology resources, 17(1):96–100, 2017.
- J. Kim, N. A. Rosenberg, and J. A. Palacios. A metric space of ranked tree shapes and ranked genealogies. bioRxiv, 2019. doi: 10.1101/2019.12.23.887125. URL <https://www.biorxiv.org/content/early/2019/12/23/2019.12.23.887125>.

- J. Kingman. The coalescent. Stochastic Processes and their Applications, 13(3):235 – 248, 1982. ISSN 0304-4149. doi: [https://doi.org/10.1016/0304-4149\(82\)90011-4](https://doi.org/10.1016/0304-4149(82)90011-4). URL <http://www.sciencedirect.com/science/article/pii/0304414982900114>.
- S. Kirkpatrick, C. D. Gelatt, and M. P. Vecchi. Optimization by simulated annealing. science, 220(4598): 671–680, 1983.
- M. K. Kuhner and J. Yamato. Practical performance of tree comparison metrics. Systematic Biology, 64(2):205–214, 12 2014.
- O. Maliet, F. Gascuel, and A. Lambert. Ranked tree shapes, nonrandom extinctions, and the loss of phylogenetic diversity. Systematic Biology, 67(6):1025–1040, 04 2018. ISSN 1063-5157. doi: 10.1093/sysbio/syy030. URL <https://doi.org/10.1093/sysbio/syy030>.
- M. Mezard and A. Montanari. Information, Physics, and Computation. Oxford University Press, 2009.
- V. N. Minin, E. W. Bloomquist, and M. A. Suchard. Smooth skyride through a rough skyline: Bayesian coalescent-based inference of population dynamics. Molecular biology and evolution, 25(7):1459–1471, 2008.
- S. A. Nadeau, T. G. Vaughan, J. Scire, J. S. Huisman, and T. Stadler. The origin and early spread of sars-cov-2 in europe. Proceedings of the National Academy of Sciences, 118(9), 2021. ISSN 0027-8424. doi: 10.1073/pnas.2012008118. URL <https://www.pnas.org/content/118/9/e2012008118>.
- J. E. O’Reilly and P. C. Donoghue. The efficacy of consensus tree methods for summarizing phylogenetic relationships from a posterior sample of trees estimated from morphological data. Systematic biology, 67(2):354–362, 2018.
- J. A. Palacios, A. Véber, L. Cappello, Z. Wang, J. Wakeley, and S. Ramachandran. Bayesian estimation of population size changes by sampling Tajima’s trees. Genetics, Early online September 11, 2019; <https://doi.org/10.1534/genetics.119.302373>, 2019. ISSN 0016-6731. doi: 10.1534/genetics.119.302373. URL <https://www.genetics.org/content/early/2019/09/11/genetics.119.302373>.
- E. Paradis and K. Schliep. ape 5.0: an environment for modern phylogenetics and evolutionary analyses in r. Bioinformatics, 35(3):526–528, 2019.
- R. Sainudiin and A. Véber. A beta-splitting model for evolutionary trees. Royal Society open science, 3(5): 160016, 2016.
- R. Sainudiin, T. Stadler, and A. Véber. Finding the best resolution for the Kingman-Tajima coalescent: theory and applications. Journal of Mathematical Biology, 70(6):1207–1247, 2015. URL <https://doi.org/10.1007/s00285-014-0796-5>.
- Y. Shu and J. McCauley. Gisaid: Global initiative on sharing all influenza data—from vision to reality. Eurosurveillance, 22(13), 2017.
- M. Slatkin and R. Hudson. Pairwise comparisons of mitochondrial DNA sequences in stable and exponentially growing populations. Genetics, 129(2):555–562, 1991.
- R. P. Stanley. Enumerative combinatorics. Volume I, 1999.

- M. A. Suchard, P. Lemey, G. Baele, D. L. Ayres, A. J. Drummond, and A. Rambaut. Bayesian phylogenetic and phylodynamic data integration using beast 1.10. Virus Evolution, 4(1), June 2018. ISSN 2057-1577. URL <https://doi.org/10.1093/ve/vey016>.
- F. Tajima. Evolutionary relationship of DNA sequences in finite populations. Genetics, 105(2):437–460, 1983.
- E. Volz, V. Hill, J. T. McCrone, A. Price, D. Jorgensen, Á. O’Toole, J. Southgate, R. Johnson, B. Jackson, F. F. Nascimento, et al. Evaluating the effects of SARS-CoV-2 spike mutation D614G on transmissibility and pathogenicity. Cell, 184(1):64–75, 2021.
- E. M. Volz, K. Koelle, and T. Bedford. Viral phylodynamics. PLoS Comput Biol, 9(3):e1002947, 2013.
- J. Wakeley. Coalescent Theory: An Introduction. Roberts & Company Publishers, June 2008. ISBN 0974707759.
- A. Willis and R. Bell. Confidence sets for phylogenetic trees. Journal of Computational and Graphical Statistics, 27(525):542–552, 2018. doi: 10.1080/01621459.2017.1395342. URL <https://doi.org/10.1080/01621459.2017.1395342>.

A Distance calculation between heterochronous trees with different sampling events

In Section ??, we stated the definitions of metrics for the case of isochronous ranked tree shapes and ranked unlabeled genealogies. Here, we detail the distance calculation for heterochronous trees with the same number of tips.

Following the notation and details of Section 3 of the appendix of Kim et al. [2019], let T_1^R, \dots, T_M^R be heterochronous ranked tree shapes with n tips, and m_1, \dots, m_M sampling events respectively. In order to compute pairwise distances, we require these trees to be represented by \mathbf{F} -matrices of the same dimension. We do this by considering the sequence of sampling and coalescent events for each tree, and inserting artificial sampling events to align the sequences of the different trees. Note that the following formulation is done going backwards in time with time increasing from the present to the past.

Here, we modified the proposed approach to increase computation speed. Instead of inserting artificial sampling events one pair at a time, we insert all artificial sampling events needed by taking all trees at once. That is, for $i = 1, \dots, m$, let $\mathbf{E}^{(i)} = (e_{m_i+n-1}^{(i)}, \dots, e_1^{(i)})$ be the vector of ordered sampling and coalescent events of tree i , where $e_{m_i+n-1}^{(i)}$ denotes the most recent sampling event ($e_{m_i+n-1}^{(i)} = s$), assumed to occur at time $u_{m_i+n-1}^{(i)} = 0$. In particular, $(e_1^{(i)} = c)$ denotes the coalescent event at time $u_1^{(i)}$ corresponding to the most recent common ancestor of the leaves in T_i^R . Each $e_j^{(i)}$ is either a sampling event ($e_j^{(i)} = s$) or a coalescent event ($e_j^{(i)} = c$). The event of type c occurs $n - 1$ times and the event of type s occurs m_i times in $\mathbf{E}^{(i)}$.

We then transform all $\mathbf{E}^{(i)}$ into extended vectors of higher dimension, in such a way that all vectors are of the same dimension and all coalescent events are position in the same entries for all trees. We first align all $n - 1$ coalescent events among all the trees by adding empty spaces when needed. Once all the type- c events are aligned, we next align the sampling events between two successive coalescent events or between $t = 0$ and the first c event. In each interval, we add additional sampling events to each tree if it has fewer than the maximum number among the different trees. We denote these by a , and assign 0 new samples to type- a events. We then construct the \mathbf{F} -matrices and their corresponding modified and extended \mathbf{W} matrices following the construction in Kim et al. [2019].

B Proof of Theorem 1

Proof. This proof builds on the Proof of Theorem 1 in the appendix of Kim et al. [2019]. We specialise to the case of isochronous trees, in which all tips are sampled at time $u_n = 0$.

We want to define the mapping between \mathcal{T}_n and \mathcal{F}_n . Consider a given ranked tree shape T with n leaves. We wish to construct F , the corresponding element of \mathcal{F}_n , and show that this mapping is a bijection.

Remember that \mathcal{F}_n is the space of $(n - 1) \times (n - 1)$ \mathbf{F} -matrices, which are lower triangular square matrices of non-negative integers that obey the following constraints:

F1 The diagonal elements are $F_{i,i} = i + 1$ for $i = 1, \dots, n - 1$ and the subdiagonal elements are $F_{i+1,i} = i$ for $i = 1, \dots, n - 2$.

F2 The elements $F_{i,1}, i = 3, \dots, n - 1$, in the first column satisfy $\max\{0, F_{i-1,1} - 1\} \leq F_{i,1} \leq F_{i-1,1}$.

F3 All the other elements $F_{i,k}, i = 4, \dots, n - 1$ and $k = 2, \dots, i - 2$ satisfy the following inequalities:

$$\max\{0, F_{i,k-1}\} \leq F_{i,k} \quad (19)$$

$$F_{i-1,k} - 1 \leq F_{i,k} \leq F_{i-1,k} \quad (20)$$

$$F_{i,k-1} + F_{i-1,k} - F_{i-1,k-1} - 1 \leq F_{i,k} \leq F_{i,k-1} + F_{i-1,k} - F_{i-1,k-1} \quad (21)$$

We first set up some notation. We view the tree as a branching process starting at the root, and ending at the time when there are n leaves. Let each internal node of the ranked tree shape be labeled with the number of branches in the tree immediately after it bifurcates, and let u_{i-1} be the time at which node i bifurcates. I.e. The root has label 2, and the last internal node has label n . Let I_i be the interval between u_i and u_{i+1} , i.e. the interval between the bifurcations of nodes $i - 1$ and i .

We define an intermediate matrix D of the same shape before defining F . Let D be an $(n - 1) \times (n - 1)$ lower triangular matrix, where D_{ij} is the number of descendants of node $j + 1$ (i.e. that were born at time u_j), that have not yet bifurcated until u_{i+1} , i.e. the end of interval I_i . We see that $D_{ij} \in \{0, 1, 2\}$, and in particular, we must also have:

D1 $D_{ii} = 2, i = 1, \dots, n - 1$.

D2 $D_{(i-1)j} - 1 \leq D_{ij} \leq D_{(i-1)j} \forall i, j$.

D3 Exactly one of the branches bifurcates at time $u_i, i = 1, \dots, n - 1$, i.e. $\forall j$,

$$\sum_{j=1}^{i-1} \mathbf{1}_{\{D_{(i-1)j} - D_{ij} = 1\}} = 1,$$

where $\mathbf{1}_P$ is the indicator function, which is 1 if P is true and 0 otherwise.

We see that this matrix D is uniquely determined for any given binary ranked tree shape T . We can reconstruct T given the matrix D by starting at the root and successively bifurcating branches according to the column of D in which we observe a difference between $D_{(i-1)j}$ and D_{ij} . This shows that the space \mathcal{T}_n is in bijection with \mathcal{D}_n , the space of matrices D that obey the conditions above. We now show that this space is in bijection with \mathcal{F}_n .

For a given matrix D , let $\varphi(D) = F$ be given by

$$F_{ij} = \sum_{k=1}^j D_{ik}.$$

The inverse mapping is $\varphi^{-1} : \mathcal{F}_n \rightarrow \mathcal{D}_n$ which is given by

$$D_{ij} = F_{ij} - F_{i(j-1)}$$

considering $F_{i0} = 0$.

In terms of T , F_{ij} denotes the total number of branches at time u_j that have not bifurcated by time u_{i+1} , i.e. the end of interval I_i . It is clear that the mapping $\varphi : D \mapsto F$ is a one-to-one mapping. We are left to show that the range of the mapping φ is exactly \mathcal{F}_n . It suffices to show that $\varphi(\mathcal{D}_n) \subseteq \mathcal{F}_n$ and $\varphi^{-1}(\mathcal{F}_n) \subseteq \mathcal{D}_n$.

Consider a matrix $D \in \mathcal{D}_n$, and $F = \varphi(D)$. After any branching event, there is one node that has split, and the rest are as they were. This translates to $\sum_{k=1}^{i-1} D_{ik} = \left(\sum_{k=1}^{i-1} D_{(i-1)k} \right) - 1$. Note F must satisfy $F_{ii} = i + 1$, as $F_{11} = D_{11} = 2$, and

$$F_{ii} = \sum_{k=1}^i D_{ik} = D_{ii} + \sum_{k=1}^{i-1} D_{ik} = 2 + \left(\sum_{k=1}^{i-1} D_{(i-1)k} \right) - 1 = F_{(i-1)(i-1)} + 1$$

We will also have $F_{(i+1)i} = i$, as

$$F_{(i+1)i} = \sum_{k=1}^i D_{(i+1)k} = \left(\sum_{k=1}^i D_{ik} \right) - 1 = F_{ii} - 1 = i$$

This shows that F satisfies condition F1.

We have $F_{i1} = D_{i1} \forall i$. This shows condition F2 using D2 for $j = 1$.

Now we come to condition F3. F3.19 follows by non-negativity and the fact that the columns of D are monotonically decreasing. F3.20 follows using D3. F3.21 is equivalent to

$$\begin{aligned} 0 &\leq (F_{(i-1)k} - F_{ik}) - (F_{(i-1)(k-1)} - F_{i(k-1)}) \leq 1 \\ \iff 0 &\leq \left(\sum_{j=1}^k D_{(i-1)j} - \sum_{j=1}^k D_{ij} \right) - \left(\sum_{j=1}^{k-1} D_{(i-1)j} - \sum_{j=1}^{k-1} D_{ij} \right) \leq 1 \\ \iff 0 &\leq D_{(i-1)k} - D_{ik} \leq 1 \end{aligned}$$

which follows from D2 and D3. This shows that $\varphi(\mathcal{D}_n) \subseteq \mathcal{F}_n$.

Now let F be an element of \mathcal{F}_n and $D = \varphi^{-1}(F)$.

We first see that $D_{ii} = F_{ii} - F_{(i-1)i} = (i + 1) - (i - 1) = 2$. This shows D1. Following the case above, we see that F3.21 implies D2, and F3.20 implies D3. This shows that $\varphi^{-1}(\mathcal{F}_n) \subseteq \mathcal{D}_n$ and completes the proof of the bijection. □

Here the expectation is taken with respect to the joint density of u , i.e. $\mathbb{E}[w_j(\mathbf{u})] = \int_{\mathbf{u}} w_j(\mathbf{u})f(\mathbf{u})d(\mathbf{u})$. We see that (25) is satisfied simultaneously for all k if we have:

$$F_j^G = \sum_{F \in \mathcal{F}_n} \mu(F)F_j = \mathbb{E}(F_j),$$

and

$$g_j(I^G) = \mathbb{E}[w_j(\mathbf{u})],$$

for $j = 1, \dots, m = n(n-1)/2$. We note that the expected value $\mathbb{E}(F)$ may not correspond to the Fréchet mean tree; although this is a solution, we are ignoring the constraints imposed to F . \square

D A Markov chain on the space of ranked tree shapes

We drop the F matrix representation of ranked tree shapes and instead use two string representations of the spaces of isochronous and heterochronous ranked tree shapes respectively. We use the string representations to define two Markov chains on the corresponding spaces. An isochronous ranked tree shape is encoded as a string of $n-1$ integers $t = (t_1, t_2, \dots, t_{n-1})$, where t_k indicates the parent node of the internal node with ranking $k+1$, $k \in \{1, \dots, n-1\}$. It is assumed that the first integer t_1 of the string representation is 1 (parent of root node). Figure 2 shows the string encodings of each of the 5 ranked tree shapes at the bottom. The string representation was introduced earlier as the functional code for binary increasing trees [Donaghey, 1975]. The set of all string representations of $n-1$ elements are in bijection with the space of isochronous ranked tree shapes of n leaves and the space of binary increasing trees of $n-1$ nodes [Stanley, 1999].

To recover the tree T from the encoding t , we can proceed in a generative fashion: we start at the root which has label 2, and proceed by bifurcating the leaves in the order determined by t . The space of strings \mathfrak{T}_n is the set of all t strings of length $n-1$ defined as follows:

Definition 10. (Isochronous string representation). A string t of non-negative integers that encodes an isochronous ranked tree shape has the following defining properties:

1. $t_1 = 1$
2. For $i > 1$, $2 \leq t_i \leq i$.
3. No entry of t can appear more than twice.

Definition 11. (Markov chain on isochronous strings). Let $t \in \mathfrak{T}_n$ be a string encoding an isochronous ranked tree shape as described in Definition 10. We define a Markov chain on \mathfrak{T}_n as follows:

1. Pick an element $i \in 2, \dots, n$ uniformly at random.
2. Pick the value of t_i uniformly at random from the allowable choices in $2, \dots, i$, i.e. from those choices that do not already appear twice among t_{-i} .

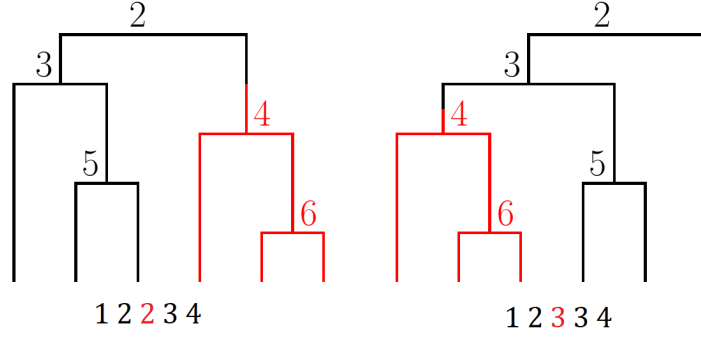


Figure 15: An example transition under the Markov chain of Definition 11 from $(1, 2, 2, 3, 4)$ to $(1, 2, 3, 3, 4)$. The subtree of node 4 is plucked from under node 2 and planted under node 3.

Proposition 12. The Markov chain on isochronous strings (Definition 11) is ergodic with uniform stationary distribution on the space of strings of length $n - 1$, or equivalently, on the space of ranked tree shapes with n leaves.

Proof. Let t be an arbitrary element of \mathfrak{T}_n . We show that t is path connected to $t^* = (1, 2, \dots, n - 1)$. This string corresponds to the most unbalanced tree, also called the caterpillar or the comb tree. Since the Markov chain is symmetric, t^* is path connected to every element of \mathfrak{T}_n as well and hence the chain is irreducible. The following path has all transitions with positive probability:

$$\begin{aligned}
 t &= t^{(0)} = (1, t_2, t_3, \dots, t_{n-2}, t_{n-1}) \\
 t^{(1)} &= (1, t_2, t_3, \dots, t_{n-2}, n - 1) \\
 t^{(2)} &= (1, t_2, t_3, \dots, n - 2, n - 1) \\
 &\vdots \\
 t^{(n-3)} &= (1, t_2, 3, \dots, n - 2, n - 1) \\
 t^{(n-2)} &= (1, 2, 3, \dots, n - 2, n - 1) = t^*
 \end{aligned}$$

Note that $t^{(i)} \mapsto t^{(i+1)}$ is always a valid transition due to Property 10.3. □

This representation can be extended to heterochronous trees as well, with additional entries indicating the sampling events. We define these strings in the following way:

Definition 13. (Heterochronous string representation). A heterochronous ranked tree shape with n leaves is encoded as a pair of strings (t, σ) each of length $2n - 1$. As before, t is a string of non-negative integers that indicates the parent nodes of internal nodes (coalescent events), however, t now also includes the parent nodes of all leaves. The sequence order is given by the time they are created and σ is a $0 - 1$ string that indicates whether the corresponding node is internal (1) or a leaf (0). These strings have the following defining properties:

1. $t_1 = 1, \sigma_1 = 1$
2. $|\{i : \sigma_i = 1\}| = n - 1$
3. $|\{i : \sigma_i = 0\}| = n$
4. Each element of $\{2, \dots, n\}$ occurs exactly twice in t .
5. For each $i > 1, 2 \leq t_i \leq 1 + \sum_{j=1}^{i-1} \sigma_j$. We note that the string $t_\sigma = (t_i : \sigma_i = 1)$ is a valid string encoding an isochronous ranked tree shape.

For example, the string representation of the ranked tree shape of Figure 1(C) is ($t = 123442365567788, \sigma = 111100101100000$). We note that the string $t_\sigma = (t_i : \sigma_i = 1)$ is a valid string encoding of an isochronous ranked tree shape. In addition, this representation can also admit extensions to multifurcating trees, which we leave for future study.

While defining Markov chains on the space of ranked tree shapes is useful for Bayesian inference in areas such as phylogenetics and phylodynamics, we rely on these chains for finding the Fréchet mean via stochastic combinatorial optimization (Section 3.3).

Definition 14. (Markov chain on heterochronous strings). Let (t, σ) be a pair of strings encoding an heterochronous ranked tree shape as described in Property 13. We define a Markov chain on the space of such strings, conditional on σ a fixed sequence of sampling and coalescent events, with transitions as follows:

1. Pick two distinct element $i, j \in 2, \dots, 2n - 1$ uniformly at random.
2. Swap t_i and t_j . If the result is a valid heterochronous string, accept the move, otherwise reject the move.

The Markov chain of Definition 14 on the space of ranked tree shapes with a given σ , i.e., with a given sequence of sampling and coalescence events, is also symmetric, aperiodic (we can pick a pair with the same label with positive probability) and irreducible. The proof of irreducibility is similar to the isochronous case by considering only the coalescent events.

Proof. Let (t, σ) be the encoding of an arbitrary heterochronous ranked tree shape.

We first define (t^*, σ) which is the analogue of the caterpillar or the most unbalanced tree, but with the given σ . Let $t_\sigma^* = (t_i^* : \sigma_i = 1)$ be equal to $(1, 2, \dots, n-1)$, and $t_{-\sigma}^* = (t_i^* : \sigma_i = 0)$ be equal to $(2, 3, \dots, n-1, n, n)$. We can follow a similar method as in the isochronous case and show that t is path connected to t^* by a sequence of steps with positive probability. Note that t has length $2n - 1$.

Let $t^{(0)} = t$. We obtain $t^{(i)}$ by swapping two terms of $t^{(i-1)}$ such that the last i terms of $t^{(i)}$ and t^* are equal. Explicitly, let j be the largest element in $2, \dots, 2n - i$ such that $t_j^{(i-1)} = t_{2n-i}^*$. We can swap $t_j^{(i-1)}$ and $t_{2n-i}^{(i-1)}$, since t_{2n-i}^* is the maximum allowable entry at position $2n - i$, and hence $t_{2n-i}^{(i-1)} \leq t_j^{(i-1)}$ which satisfies Definition 13.5. The remaining conditions under Definition 13 are not affected by the transitions. Iteratively, we obtain $t^{(2n-1)} = t^*$.

Since the Markov chain is symmetric, we see that t^* will be path connected to every t as well, and the Markov chain is irreducible. □

E Proof of Theorem 8

Proof. 1. This follows by the Markovian property of the Yule model, since the i -th row of the \mathbf{F} -matrix is only determined by the state of the tree when it has $i + 1$ tips.

2. View P as the Yule model, in which we start with one leaf, and successively bifurcate an independently chosen leaf at random. Let $D_{i,j}$ be the number of branches that were created after the j -th split (i.e. when the node with label $(j + 1)$ bifurcates), that have not bifurcated by interval i . We must have $D_{ij} \in \{0, 1, 2\}$, and $F_{ij} = \sum_{k \leq j} D_{ik}$.

We have $D_{11} = F_{11} = 2$, and $D_{i1} = F_{i1} \in \{0, 1\}$ for $i > 1$.

For the children of node 2, i.e. when $j = 1$, $D_{ij} = 1$ means that the extant branch descending from node 2 has not bifurcated yet by interval i . Since at each step in the Yule model, the branch to split is chosen at random, we have

$$P(D_{i1} = 1) = \frac{2}{3} \times \frac{3}{4} \times \cdots \times \frac{i-2}{i-1} \times \frac{i-1}{i} = \frac{2}{i} \quad (26)$$

This implies

$$E[D_{i1}] = P(D_{i1} = 1) = \frac{2}{i} \quad (27)$$

Let $j > 1$. Then $D_{ij} = 2$ means that neither of the branches descending from node $(j + 1)$ have bifurcated by interval i . By the same argument as above,

$$P(D_{ij} = 2) = \frac{j-1}{j+1} \times \frac{j}{j+2} \times \cdots \times \frac{i-3}{i-1} \times \frac{i-2}{i} = \frac{j(j-1)}{i(i-1)} \quad (28)$$

Now $D_{ij} = 1$ means that exactly one branch descending from node $(j + 1)$ has bifurcated by interval i . We split this up according to the interval where this bifurcation occurs:

$$\begin{aligned} P(D_{ij} = 1) &= \sum_{k=1}^{i-j} P(D_{ij} = 1, D_{(j+k-1)j} - D_{(j+k)j} = 1) \\ &= \sum_{k=1}^{i-j} \left(\prod_{l=1}^{k-1} \frac{j+l-2}{j+l} \right) \times \frac{2}{j+k} \times \left(\prod_{l=k+1}^i \frac{j+l-1}{j+l} \right) \\ &= \sum_{k=1}^{i-j} \frac{2j(j-1)}{i} \frac{1}{(j+k-2)(j+k-1)} \\ &= \frac{2j(i-j)}{i(i-1)} \end{aligned} \quad (29)$$

We thus have

$$\begin{aligned} P(D_{ij} = 0) &= 1 - P(D_{ij} = 1) - P(D_{ij} = 2) \\ &= \frac{(i-j)(i-j-1)}{i(i-1)} \end{aligned} \quad (30)$$

and

$$\begin{aligned} E[D_{ij}] &= P(D_{ij} = 1) + 2P(D_{ij} = 2) \\ &= \frac{2j(i-j)}{i(i-1)} + 2\frac{j(j-1)}{i(i-1)} \\ &= \frac{2j}{i} \end{aligned} \quad (31)$$

So

$$E[F_{ij}] = \sum_{k \leq j} E[D_{ik}] = \frac{j(j+1)}{i} \quad (32)$$

3. Similar to Janson et al. [2011], we will use indicator variables tracking whether a specific external branch is still present at each time interval. We will start by arbitrarily labeling the leaves and define $Z_{i,k}$ as the indicator random variable that leaf i is still present when there are k branches, when viewing it as a Tajima coalescent process, starting with n leaves and successively merging two at a time. Then $F_{n-1,k-1} = \sum_{i=1}^n Z_{i,k}$ and for $k \leq l$,

$$\text{Cov}(F_{n-1,k-1}, F_{n-1,l-1}) = \sum_{i=1}^n \sum_{j=1}^n \text{Cov}(Z_{i,k}, Z_{j,l}), \quad (33)$$

where

$$\text{Cov}(Z_{i,k}, Z_{j,l}) = E(Z_{i,k}Z_{j,l}) - E(Z_{i,k})E(Z_{j,l}) \quad (34)$$

$$E(Z_{i,k}Z_{j,l}) = P(Z_{i,k} = Z_{j,l} = 1) \quad (35)$$

is the probability that the external branch with label i and the external branch with label j remain external branches when there are k and l branches respectively. That is, the probability that leaves i and j do not coalesce when there are $n, n-1, \dots, l$ branches and when one of them do not coalesce when there are $l-1, \dots, k$. That is

$$E(Z_{i,k}Z_{j,l}) = P(Z_{i,k} = Z_{j,l} = 1) = \frac{\binom{n-2}{2} \binom{n-3}{2} \dots \binom{l-1}{2} \binom{l-1}{2} \dots \binom{k}{2}}{\binom{n}{2} \binom{n-1}{2} \dots \binom{l+1}{2} \binom{l}{2} \dots \binom{k+1}{2}} = \frac{(l-1)(l-2)k(k-1)}{n(n-1)^2(n-2)}, \quad (36)$$

and

$$E(Z_{i,k}) = P(Z_{i,k} = 1) = \frac{\binom{n-1}{2} \binom{n-2}{2} \dots \binom{k}{2}}{\binom{n}{2} \binom{n-1}{2} \dots \binom{k+1}{2}} = \frac{k(k-1)}{n(n-1)}, \quad (37)$$

$$\text{Var}(Z_{i,k}) = \frac{k(k-1)}{n(n-1)} \left(1 - \frac{k(k-1)}{n(n-1)} \right), \quad (38)$$

$$\begin{aligned}
\text{Cov}(Z_{i,k}Z_{j,l}) &= \frac{(l-1)(l-2)k(k-1)}{n(n-1)^2(n-2)} - \frac{k(k-1)l(l-1)}{n^2(n-1)^2} \\
&= \frac{(l-1)(k-1)k}{n(n-1)^2} \left[\frac{l-2}{n-2} - \frac{l}{n} \right] \\
&= \frac{-2(n-l)(l-1)k(k-1)}{n^2(n-1)^2(n-2)}
\end{aligned} \tag{39}$$

$$\begin{aligned}
\text{Cov}(Z_{1,i}, Z_{2,i}) &= \text{E}(Z_{1,i}Z_{2,i}) - \text{E}(Z_{1,i})\text{E}(Z_{2,i}) \\
&= \frac{\binom{i}{2}\binom{i-1}{2}}{\binom{n}{2}\binom{n-1}{2}} - \frac{i^2(i-1)^2}{n^2(n-1)^2} = \frac{-2i(i-1)^2(n-i)}{n^2(n-1)^2(n-2)}
\end{aligned} \tag{40}$$

and

$$\begin{aligned}
\text{Var}(F_{n-1,i-1}) &= \sum_{j=1}^n \text{Var}(Z_{j,i}) + n(n-1)\text{Cov}(Z_{1,i}, Z_{2,i}) \\
&= \frac{i(i-1)}{n-1} \left(1 - \frac{i(i-1)}{n(n-1)} \right) + \frac{-2i(i-1)^2(n-i)}{n(n-1)(n-2)} \\
&= \frac{i(i-1)}{n(n-1)^2(n-2)} [n(n-1)(n-2) - i(i-1)(n-2) - 2(i-1)(n-i)(n-1)] \\
&= \frac{i(i-1)}{n-1} - \frac{i(i-1)^2}{n(n-1)^2(n-2)} [i(n-2) + 2(n-i)(n-1)] \\
&= \frac{i(i-1)}{n-1} - \frac{i^2(i-1)^2}{n(n-1)^2} - \frac{2i(i-1)^2(n-i)}{n(n-1)(n-2)} \\
&= \frac{i^2(i-1)^2}{(n-1)^2(n-2)} + \frac{i(i-1)(n-2i)}{(n-1)(n-2)}
\end{aligned} \tag{41}$$

So

$$\text{Var}[F_{ij}] = \frac{j^2(j+1)^2}{i^2(i-1)} + \frac{j(j+1)(i-2j-1)}{i(i-1)}$$

4. We continue to show the results of covariance. First, when $k \leq l$

$$\begin{aligned}
\text{Cov}(F_{n-1,k-1}, F_{n-1,l-1}) &= \sum_{i=1}^n \sum_{j=1}^n \text{Cov}(Z_{i,k}, Z_{j,l}) = n(n-1)\text{E}(Z_{1,k}Z_{2,l}) + n\text{E}(Z_{1,k}) - n^2\text{E}(Z_{1,k})\text{E}(Z_{1,l}) \\
&= \frac{(l-1)(l-2)k(k-1)}{(n-1)(n-2)} + \frac{k(k-1)}{n-1} - \frac{k(k-1)l(l-1)}{(n-1)^2} \\
&= \frac{k(k-1)[l(l+1) + n(n-2l-1)]}{(n-1)^2(n-2)}
\end{aligned} \tag{42}$$

So when $i_1 = i_2, j_1 \leq j_2$,

$$\text{Cov}[F_{i_1 j_1}, F_{i_2 j_2}] = \frac{j_1(j_1 + 1)[j_2(j_2 + 2) + (i_1 + 1)(i_1 - 2j_2 - 2)]}{i_1^2(i_1 - 1)}$$

Now, when comparing values of the \mathbf{F} matrix at different rows, for example $F_{n-1, k-1}$ and $F_{m-1, k-1}$ for $k < n < m$, we then assume that $F_{m-1, k-1} = \sum_{i=1}^m Z_{i, k}$ denotes the number of external branches in a ranked tree shape with m leaves when there are k branches as before, however, when considering it together with $F_{n-1, k}$, $F_{n-1, k}$ denotes the number of external branches when there are k branches in a ranked tree shape with n leaves. That is, when there are n branches, there are $\sum_{i=1}^m Z_{i, n}$ external branches with respect to the bigger tree but there are additional $n - \sum_{i=1}^m Z_{i, n}$ branches that are external with respect to the smaller tree. We then have

$$\begin{aligned} \text{Cov}(F_{m-1, k-1}, F_{n-1, k-1}) &= \text{Cov}\left(F_{m-1, k-1}, F_{m-1, k-1} + \sum_{j=m+1}^{2m-n} Z_{j, k}\right) \\ &= \text{Var}(F_{m-1, k-1}) + m \sum_{j=m+1}^{2m-n} \text{Cov}(Z_{1, k}, Z_{j, k}) \end{aligned} \quad (43)$$

where

$$\begin{aligned} \text{Cov}(Z_{1, k}, Z_{m+1, k}) &= E[Z_{1, k} Z_{m+1, k}] - E[Z_{1, k}]E[Z_{m+1, k}] \\ &= \frac{\binom{m-1}{2} \binom{m-3}{2} \dots \binom{k}{2} \binom{k-1}{2}}{\binom{m}{2} \binom{m-1}{2} \dots \binom{k+2}{2} \binom{k+1}{2}} - \frac{\binom{k}{2} \binom{k}{2}}{\binom{m}{2} \binom{m-1}{2}} \\ &= \frac{\binom{k}{2} \binom{k-1}{2}}{\binom{m}{2} \binom{m-2}{2}} - \frac{\binom{k}{2} \binom{k}{2}}{\binom{m}{2} \binom{m-1}{2}} \\ &= \frac{k(k-1)^2(k-2)}{m(m-1)(m-2)(m-3)} - \frac{k^2(k-1)^2}{m(m-1)^2(m-2)} \end{aligned} \quad (44)$$

$$\begin{aligned} \text{Cov}(Z_{1, k}, Z_{m+2, k}) &= \frac{\binom{m-1}{2} \binom{m-2}{2} \binom{m-4}{2} \dots \binom{k}{2} \binom{k-1}{2}}{\binom{m}{2} \binom{m-1}{2} \binom{m-2}{2} \dots \binom{k+2}{2} \binom{k+1}{2}} - \frac{\binom{k}{2} \binom{k}{2}}{\binom{m}{2} \binom{m-2}{2}} \\ &= \frac{\binom{k}{2} \binom{k-1}{2}}{\binom{m}{2} \binom{m-3}{2}} - \frac{\binom{k}{2} \binom{k}{2}}{\binom{m}{2} \binom{m-2}{2}} \\ &= \frac{k(k-1)^2(k-2)}{m(m-1)(m-3)(m-4)} - \frac{k^2(k-1)^2}{m(m-1)(m-2)(m-3)} \end{aligned} \quad (45)$$

and

$$\begin{aligned} \sum_{j=m+1}^{2m-n} \text{Cov}(Z_{1, k}, Z_{j, k}) &= \sum_{l=2}^{m-n+1} \left\{ \frac{k(k-1)^2(k-2)}{m(m-1)(m-l)(m-l-1)} - \frac{k^2(k-1)^2}{m(m-1)(m+1-l)(m-l)} \right\} \\ &= \frac{k(k-1)^2(k-2)(m-n)}{m(m-1)(m-2)(n-2)} - \frac{k^2(k-1)^2(m-n)}{m(m-1)^2(n-1)} \end{aligned}$$

$$= \frac{k(k-1)^2(m-n)}{m(m-1)} \left[\frac{k-2}{(m-2)(n-2)} - \frac{k}{(m-1)(n-1)} \right] \quad (46)$$

Therefore,

$$\begin{aligned} \text{Cov}(F_{m-1,k-1}, F_{n-1,k-1}) &= \frac{k^2(k-1)^2}{(m-1)^2(m-2)} + \frac{k(k-1)(m-2k)}{(m-1)(m-2)} \\ &\quad + \frac{k(k-1)^2(m-n)}{(m-1)} \left[\frac{k-2}{(m-2)(n-2)} - \frac{k}{(m-1)(n-1)} \right] \\ &= \frac{k(k-1)(k-n)(k-n+1)}{(m-1)(n-1)(n-2)} \end{aligned} \quad (47)$$

So when $i_1 > i_2, j_1 = j_2$,

$$\text{Cov}[F_{i_1 j_1}, F_{i_2 j_2}] = \frac{j_2(j_2+1)(j_2-i_2)(j_2-i_2+1)}{i_1 i_2 (i_2-1)}$$

For $i < j, i < n$ and $j < m$

$$\begin{aligned} \text{Cov}(F_{n-1,i-1}, F_{m-1,j-1}) &= \text{Cov}(F_{m-1,i,-1} + \sum_{l=m+1}^{2m-n} Z_{l,i}, F_{m-1,j-1}) \\ &= \text{Cov}(F_{m-1,i,-1}, F_{m-1,j-1}) + \text{Cov}(F_{m-1,j-1}, \sum_{l=m+1}^{2m-n} Z_{l,i}) \end{aligned} \quad (48)$$

where

$$\begin{aligned} \text{Cov}(F_{m-1,j-1}, \sum_{l=m+1}^{2m-n} Z_{l,i}) &= m(m-n)\text{Cov}(Z_{1,j}, Z_{m+1,i}) \\ &= m(m-n) \left[\text{E}[Z_{1,j}Z_{m+1,i}] - \frac{j(j-1)}{m(m-1)} \frac{i(i-1)}{n(n-1)} \right] \\ &= m(m-n) \left[\frac{(j-1)(j-2)}{m(m-1)} \frac{i(i-1)}{(n-1)(n-2)} - \frac{j(j-1)}{m(m-1)} \frac{i(i-1)}{n(n-1)} \right] \\ &= \frac{(m-n)(j-1)i(i-1)}{(m-1)(n-1)} \left[\frac{j-2}{n-2} - \frac{j}{n} \right] \end{aligned} \quad (49)$$

Then, for $i < j, i < n, j < m$, and $m > n$

$$\text{Cov}(F_{n-1,i-1}, F_{m-1,j-1}) = \frac{i(i-1)[j(j+1) + m(m-2j-1)]}{(m-1)^2(m-2)} + \frac{(m-n)(j-1)i(i-1)}{(m-1)(n-1)} \left[\frac{j-2}{n-2} - \frac{j}{n} \right] \quad (50)$$

So when $i_1 > i_2, j_1 > j_2$,

$$\text{Cov}[F_{i_1 j_1}, F_{i_2 j_2}] = \frac{j_2(j_2 + 1)[(j_1 + 1)(j_1 + 2) + (i_1 + 1)(i_1 - 2j_1 - 2)]}{i_1^2(i_1 - 1)} + \frac{(i_1 - i_2)j_1 j_2(j_2 + 1)}{i_1 i_2} \left[\frac{j_1 - 1}{i_2 - 1} - \frac{j_1 + 1}{i_2 + 1} \right]$$

Now, for $j < i, i < n, j < m$, and $m > n$

$$\begin{aligned} \text{Cov}(F_{n-1, i-1}, F_{m-1, j-1}) &= \text{Cov}(F_{m-1, i-1} + \sum_{l=m+1}^{2m-n} Z_{l, i}, F_{m-1, j-1}) \\ &= \text{Cov}(F_{m-1, i-1}, F_{m-1, j-1}) + \text{Cov}(F_{m-1, j-1}, \sum_{l=m+1}^{2m-n} Z_{l, i}) \end{aligned} \quad (51)$$

where

$$\begin{aligned} \text{Cov}(F_{m-1, j-1}, \sum_{l=m+1}^{2m-n} Z_{l, i}) &= m(m-n)\text{Cov}(Z_{1, j}, Z_{m+1, i}) \\ &= m(m-n) \left[\text{E}[Z_{1, j} Z_{m+1, i}] - \frac{j(j-1)}{m(m-1)} \frac{i(i-1)}{n(n-1)} \right] \\ &= m(m-n) \left[\frac{(i-1)(i-2)}{m(m-1)} \frac{j(j-1)}{(n-1)(n-2)} - \frac{j(j-1)}{m(m-1)} \frac{i(i-1)}{n(n-1)} \right] \\ &= \frac{(m-n)(j-1)j(i-1)}{(m-1)(n-1)} \left[\frac{i-2}{n-2} - \frac{i}{n} \right] \end{aligned} \quad (52)$$

Then, for $j < i, i < n, j < m$, and $m > n$:

$$\text{Cov}(F_{n-1, i-1}, F_{m-1, j-1}) = \frac{j(j-1)[i(i+1) + m(m-2i-1)]}{(m-1)^2(m-2)} + \frac{(m-n)(j-1)j(i-1)}{(m-1)(n-1)} \left[\frac{i-2}{n-2} - \frac{i}{n} \right] \quad (53)$$

So when $i_1 > i_2, j_1 < j_2$,

$$\text{Cov}[F_{i_1 j_1}, F_{i_2 j_2}] = \frac{j_1(j_1 + 1)[(j_2 + 1)(j_2 + 2) + (i_1 + 1)(i_1 - 2j_2 - 2)]}{i_1^2(i_1 - 1)} + \frac{(i_1 - i_2)j_1(j_1 + 1)j_2}{i_1 i_2} \left[\frac{j_2 - 1}{i_2 - 1} - \frac{j_2 + 1}{i_2 + 1} \right]$$

□

F Temperature schedules for Simulated Annealing

We now consider the choice of temperature schedule in the Simulated Annealing (SA) algorithm of Section 3.3. in the main document. The parameters to be chosen are whether we use a logarithmic, linear, or

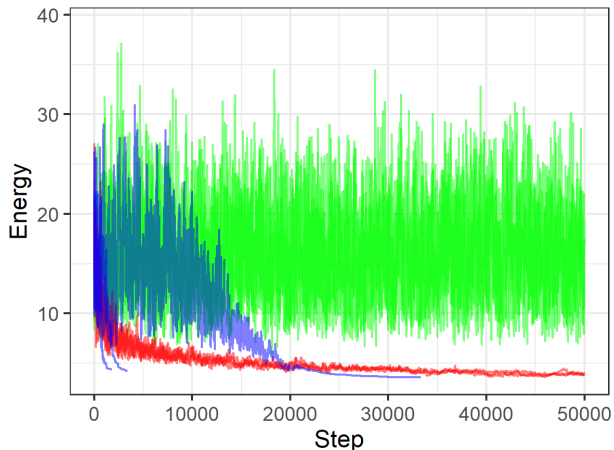


Figure 16: Example energy runs a simulated annealing chain, with trees on $n = 100$ tips. Three runs each for the logarithmic (green), linear (red), and exponential (blue) schedules. We observe that the exponential schedule with $\alpha = .9995$ has the best performance.

exponential cooling regime, as well as the initial temperature R_0 , and cooling rate α . Theoretical convergence guarantees exist for the logarithmic cooling schedule $R_k = R_0(1 + \alpha \log(1 + k))^{-1}$ with sufficiently high initial temperature and appropriately chosen α (see Chapter 3 of Aarts and Korst [1988]). Other options include the linear schedule $R_k = R_0(1 + \alpha k)^{-1}$, or the exponential cooling schedule $R_k = R_0\alpha^k$. In practice, the logarithmic schedule is very inefficient and better choices may be made for each different problem.

In our simulations, we observed that the exponential cooling schedule with $\alpha = .9995$ works well for trees with upto $n = 250$ tips. We note the logarithmic schedule is prohibitively slow, and we do not gain much by using the linear schedule over the exponential schedule.

G SARS-CoV-2 Posterior Inference and Sample Information

We accessed a global alignment of SARS-CoV-2 publicly available molecular sequences obtained from infected human individuals on November 4, 2020 in the GISAID EpiCov database [Shu and McCauley, 2017]. We analyzed a subset of available sequences sampled in the states of California, Florida, Texas and Washington in the USA for the period of February 2020 to September 2020. We analyzed 19 random samples of 100 sequences in California and 3 random samples of 100 sequences in the rest of the states. We independently sampled genealogies from the posterior distribution for each random sample independently with BEAST [Suchard et al., 2018]. In BEAST, we placed the HKY mutation prior on the substitution process with fixed global mutation rate of 8×10^{-4} substitutions per site per year as it has been done in other studies [Nadeau et al., 2021], and we placed the Skyride process prior on the coalescent effective population size [Minin et al., 2008]. We ran each chain for 50 million iterations and thinned every 5000 iterations.

We acknowledge the following submitting and originating laboratories that made the sequences used in this manuscript available in GISAID: San Diego County Public Health Laboratory, Quest Diagnostics, UCLA Pathology Clinical Microbiology Lab, Cedars-Sinai Medical Center, Department of Pathology & Laboratory

Medicine, Molecular Pathology Laboratory, San Joaquin County Public Health Lab, Orange County Public Health Laboratory, UCSF Clinical Microbiology Laboratory, UC San Diego Center for Advanced Laboratory Medicine, County of Santa Clara Public Health, Scripps Medical Laboratory, California Department of Public Health, Ventura County Public Health Lab, Rady's Childrens Hospital, Stanford clinical virology lab, Santa Clara County Public Health Department, County of Santa Clara Public Health Department, Humboldt County Public Health Laboratory, Department of Immunology, Contra Costa Public Health Lab, San Francisco Public Health Laboratory, National Institute for Communicable Disease Control and Prevention (ICDC) Chinese Center for Disease Control and Prevention (China CDC), Innovative Genomics Institute, UC Berkeley, San Bernardino County Public Health Lab, Alameda County Public Health Lab, California Department of Health, County Of San Luis Obispo Public Health Laboratory, University of California, Davis, Andersen Lab, Microbial Diseases Laboratory, University of Wisconsin-Madison AIDS Vaccine Research Laboratories, OHSU Lab Services Molecular Microbiology Lab, San Luis Obispo Public Health Department, Tuolumne County Public Health, FL Bureau of Health Laboratories Tampa, Florida Bureau of Public Health Laboratories, Florida Department of Health, Public Health, United States Air Force School of Aerospace Medicine, University of Florida, FL Bureau of Public Health Laboratories-Miami, University of Miami Immunology and Histocompatibility Laboratory, FL Bureau of Public Health Laboratories, Laboratory of Dr. John Lednicky, Environmental and Global Health, University of Florida - Gainesville, FL Bureau of Public Health Laboratories-Tampa, Mayo Clinic Laboratories, University of Florida, FL Bur. of Public Health Laboratories-Jacksonville, Emerging Pathogens Institute, University of Florida, Environmental and Global Health, Texas DSHS Lab Services, Houston Methodist Hospital, Texas Department of State Health Services, LSUHS Emerging Viral Threat Laboratory, Texas Department of State Health Services (TXDSHS), Baylor College of Medicine, City of El Paso Department of Public Health Laboratory, Washington State Department of Health, University of Washington Virology Lab, WA State Department of Health, University of Washington, Laboratory Medicine, Laboratory Medicine, University of Washington, Washington State Public Health Lab, Harborview Medical Center, Andersen lab at Scripps Research, Kruglyak Lab, Cedars-Sinai Medical Center, Molecular Pathology Laboratory of Department of Pathology & Laboratory Medicine and Genomic Core, Chan-Zuckerberg Biohub, Chiu Laboratory, University of California, San Francisco, Q Squared Solutions - QRTP facility, Pathogen Discovery, Respiratory Viruses Branch, Division of Viral Diseases, Centers for Disease Control and Prevention, Oregon SARS-CoV-2 Genome Sequencing Center, Ginkgo Bioworks Clinical Laboratory, University of Florida, Microbial Genome Sequencing Center.